Simulation and Network Analysis of Nanoparticles Agglomeration and Structure Formation with Application to Fuel Cell Catalyst Inks

by

Razzi Movassaghi Jorshari
B.Sc., Sharif University of Technology, 2008
M.Sc., University of Victoria, 2012

A Dissertation Submitted in Partial Fulfillment of the Requirements for the Degree of

DOCTOR OF PHILOSOPHY

in the Department of Mechanical Engineering

© Razzi Movassaghi Jorshari, 2019
University of Victoria

All rights reserved. This dissertation may not be reproduced in whole or in part, by photocopying or other means, without the permission of the author.

Simulation and Network Analysis of Nanoparticles Agglomeration and Structure Formation with Application to Fuel Cell Catalyst Inks

by

Razzi Movassaghi Jorshari
B.Sc., Sharif University of Technology, 2008
M.Sc., University of Victoria, 2012

Supervisory Committee

Dr. Ned Djilali, Supervisor
(Department of Mechanical Engineering)

Dr. Peter Oshkai, Departmental Member
(Department of Mechanical Engineering)

Dr. Irina Paci, Outside Member
(Department of Chemistry)

Supervisory Committee

Dr. Ned Djilali, Supervisor
(Department of Mechanical Engineering)

Dr. Peter Oshkai, Departmental Member
(Department of Mechanical Engineering)

Dr. Irina Paci, Outside Member
(Department of Chemistry)

ABSTRACT

Agglomeration of nanoparticles occurs in a number of colloidal systems related, for example, to material processing and drug delivery. The present work is motivated by the need to improve fundamental understanding of the agglomeration and structure formation processes that occur in catalyst inks used for the fabrication of polymer electrolyte fuel cells (PEMFCs). Particle dynamics simulations are performed to investigate agglomeration under various conditions. The interaction between particles is defined using realistic physical potentials, rather than commonly used potential models, and a novel analysis of the agglomeration and structure formation process is performed using network science concepts. The simulated systems correspond to catalyst inks consisting primarily of carbon nanoparticles in solution. The effect of various conditions such as different force magnitude, shape of the force function, concentration etc. are investigated in terms of network science parameters such as average degree and shortest path. An "agglomeration timescale" and a "restructuring timescale" introduced to interpret the evolution of the agglomeration process suggest that the structure, which has a strong impact on the performance of the eventual catalyst layer, can be controlled by tuning the rate at which particles are added based on the restructuring timescale.

Table of Contents

Bibliography **90**

List of Figures

ACKNOWLEDGEMENTS

I would like to thank:

My supervisor, Dr. Ned Djilali,
My supervisory committee,
All the members of the ESTP Lab,
All the office staff at IESVic,
All the faculty members and office staff in the Mechanical Engineering Department of UVic,
and last but not least, all my friends and family.

This work could not have been done without your help and support.

DEDICATION

To my parents, my sister, my brother, and my wife.

Chapter 1

Background and Motivation

Following the invention of the internal combustion engine, petroleum became the most important source of energy in human society. However, the extraction, transport, processing and use of petroleum and its derivatives causes pollution and greenhouse gas emissions. Thus, a shift to more "environmentally friendly" resources and energy conversion technologies is essential. "Fuel cell technology" is one of the most promising ones.

A fuel cell is a device that converts the chemical energy of a fuel to the electricity via an electrochemical process. When hydrogen is used as the fuel in conjunction with oxygen as an oxidant, the only chemical by-product is water which makes the fuel cell a "clean" technology. Moreover, the electrochemical energy conversion process provides much higher efficiency than combustion. Fuel cells can also be used in a variety of applications such as transportation, portable devices, and stationary systems. These features make fuel cells a very promising candidate for long term sustainability in transportation and stationary applications, and thus, the global interest is shown by both industrial developers and governments to develop fuel cell technology.

In proton exchange membrane (PEM, also called polymer electrolyte membrane) fuel cells, hydrogen is the energy carrier or fuel of choice. Hydrogen has a high energy density and produces no green house gases when it reacts with oxygen (either electrochemically or by combustion), but though abundant as an element in nature, it has to be "extracted" through various processes discussed below. Hydrogen can be stored in different forms (physical storage in the the form of gas or liquid, or chemical storage using for example metal hybrids) for long periods of time, and can be transported

over long distances. This makes hydrogen a good energy carrier candidate (Turner, 2004; Scott, 2008).

Today, the majority of hydrogen production is from natural gas steam reforming, oil reforming, or coal gasification (Muradov and Veziroglu, 2005) which are not renewable and environmentally friendly production methods. However, hydrogen can also be produced through clean methods such as electrolysis or biomass. When the source of energy for these methods is renewable (such as wind or solar), the hydrogen production process becomes renewable and environmentally friendly, often referred to as "green hydrogen production".

Thus, sustainable and clean production of hydrogen as a fuel is possible, and despite the challenges for developing related infrastructures and end-use technologies (which require investments and improvements in technology), environmentally friendly hydrogen technologies are expected to play a major role in the future of a sustainable energy supply.

Figure 1.1 shows a schematic illustration of a proton exchange membrane (PEM) fuel cell. A fibrous gas diffusion layer (GDL) allows the distribution of the reactant gases to the catalyst layer (CL). CL is the heart of the fuel cell since the electrochemical reactions occur there. At the anode side, hydrogen is oxidized, while oxygen is reduced at the cathode side. The polymer electrolyte membrane, which separates anode and cathode, is only conductive to ions (protons in this case), and not electrons. Thus, the released electrons at the anode have to flow through an external circuit, and useful electric power is generated. Released electrons at the anode eventually recombine with protons on the cathode side to produce water. Figure 1.2 provides a good illustration of the cathode side of the membrane electrode assembly.

All the electrochemical reactions in fuel cells happen in the catalyst layer, and these reactions are facilitated by catalysts at both anode and cathode. In PEM fuel cells (which are best suited for automotive applications), the best performance is obtained by relying on platinum based catalyst layers.

Despite much progress in recent years, the performance and cost of fuel cells still requires improvements to become commercially successful. In the following section, we discuss in particular the needs for improvement of CL performance, and how this is related to the structure of CL and its fabrication processes.

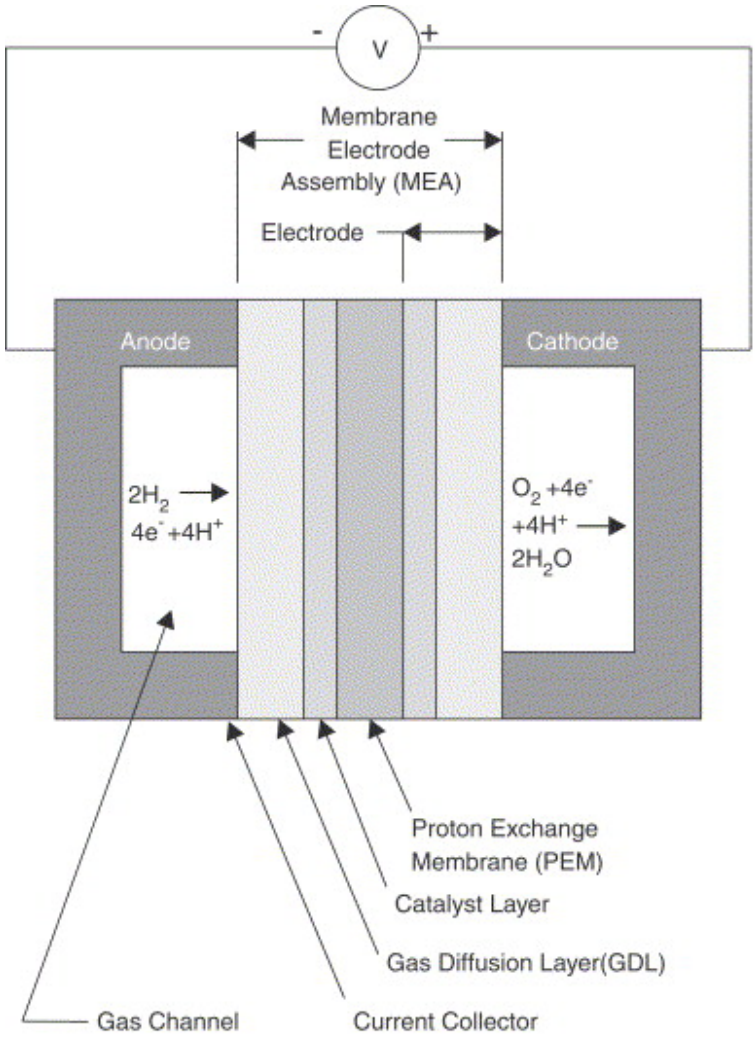

Figure 1.1: Schematic of a PEM fuel cell. Reproduced from Djilali (2007).

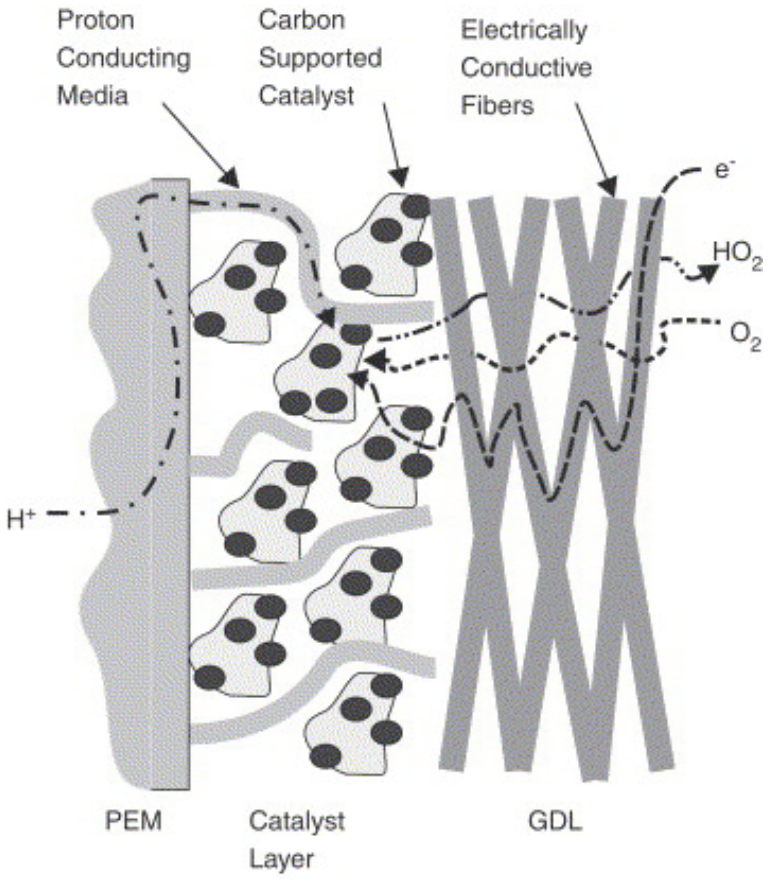

Figure 1.2: Transport of reactants, charged species and products in the cathode side of a PEM fuel cell. Reproduced from Djilali (2007).

1.1 Improvement of Catalyst Layer Performance

The main challenges for commercializing fuel cells are cost and durability. As the heart of the fuel cell, catalyst layer plays a vital role in both issues. CLs are fabricated using empirically developed methods relying on the mixing of the component materials in the form of an ink, and the application and drying of the ink that result in the nanostructured CL. To date, CL fabrication procedures have been developed largely on the basis of trial and error. Thus, the optimization of the catalyst layer performance has been hindered by the lack of fundamental knowledge regarding the fabrication and nanostructure formation processes. Given that the CL is a key operational component and that it accounts for approximately 25 to 40 % of a stack cost, depending on production volumes (Huya-Kouadio, 2017), any improvement on CL performance can help the commercial competitiveness of PEMFCs.

A major factor in the cost of a fuel cell stack is the usage of Pt as the catalyst in CLs. As has been mentioned, all the electrochemical reactions in a fuel cell happen in CL, and Pt nanoparticles (as the catalyst) are the reaction sites. Despite the significant progress during the last couple of decades, platinum utilization is still a few times higher than benchmarks for a competitive cost target (Gröger *et al.*, 2015). Thus, a more efficient usage of catalysts is required to improve fuel cell performance and reduce total cost.

The performance of CL depends on several parameters that need to be balanced and optimized simultaneously (Wilson and Gottesfeld, 1992; Secanell *et al.*, 2007, 2008). One should ensure that sufficient fuel and oxidant can reach the reaction sites (this is referred to as the "mass transport" problem), and that an effective conductivity of electrons and protons is also guaranteed. A key structural feature that affects performance is the presence of agglomerates that result in a roughly bimodal distribution of pore sizes between primary and secondary pores (Cetinbas *et al.*, 2018).

Catalyst layer is fabricated from a catalyst ink. Recently, neutron scattering based observations have shown that agglomerates that are formed in the CL ink are retained afterwards during drying process (Kusano *et al.*, 2015). These agglomerates eventually form the solid structure of the CL, and their number and size play a key role in the final electrode active area and transport properties (Siddique and Liu, 2010; Sadeghi *et al.*, 2014).

Thus, the structure of CL is strongly effected by the agglomerates that

are formed during CL ink preparations, and these agglomerates later on determine in part the solid porous nanostructure of CLs. Generally, if these agglomerates form a CL structure with higher porosity, a higher rate of mass transport will be possible, however, high porosity can be detrimental to ionic and electronic transport resulting in higher ohmic losses (Secanell *et al.*, 2007).

A well structured CL increases Pt utilization by exposing more Pt particles to the fuel. This can help to reduce the cost of the fuel cell. Pt nanoparticles (with the size range of $2 - 5$ nm (Malek *et al.*, 2007; Cheng *et al.*, 2010; Takahashi and Kocha, 2010; Xiao *et al.*, 2012)) are on the surface of (spherical) carbon nanoparticles (with a typical size of 40 nm in diameter). When carbon particles agglomerate and form very dense agglomerations (with not much space between carbon particles), many of the Pt particles will be "buried". The fuel/oxidant cannot reach these catalysts sites, and they become inactive. This is not in favor of reducing the cost of fuel cell fabrication.

Besides cost, durability (Hu *et al.*, 2009; Singh *et al.*, 2018) is also another key issue in commercialization of PEM fuel cells. The current lifetime of a fuel cell stacks is around 3500 hours, however, the target is around 5500 hours (Eberle *et al.*, 2012). Thus, significant improvement on this issue is still required.

While the CL structure is a key factor on mass transport and Pt utilization, the durability of CL also depends in part on CL structure. As fuel cell operates, the structure of CL changes over its lifetime (Borup *et al.*, 2007). The durability of CL structures depends on the composition and structure determined in part during CL ink preparation, and how they will change under long term operations. For example, while a dense structure with low porosity can not guarantee a high CL performance, a highly porous but fragile CL structure that cannot retain its structure under long term operation conditions is not also a good candidate for a fuel cell engine. Thus, a balance in structure's design is required to guarantee the high performance of CL as well as its durability.

One should note that in this work, we focus on the structural properties of CL, mainly by studying the agglomeration of carbon nanoparticles during ink preparation. There are other factors related to performance of CL which are outside the scope of this work; for example, the degradation of platinum due to elctrochemical or chemical phenomena. Such degradation happens when platinum particles in CL dissolve, redeposit, coagulate, or detach as fuel

cell operates (Shao-Horn *et al.*, 2007; Meier *et al.*, 2014; Xing *et al.*, 2014; Cherevko *et al.*, 2016; Monz *et al.*, 2016; Baroody *et al.*, 2018). There are also other mechanisms that can affect CL performance such as poisoning of catalyst particles due to presence of contaminants (such as carbon monoxide, CO) (Baschuk and Li, 2001; Li *et al.*, 2003) and carbon corrosion (Hu *et al.*, 2009).

Another important point is that the main limitations on improving CL performance is for cathode side of the fuel cell because the kinetics of the reaction at the cathode (reduction of oxygen) is orders of magnitude slower than hydrogen oxidation at the anode (Li *et al.*, 2008). Moreover both electrons and protons must be conducted effectively from anode to cathode to ensure the reaction happen with minimal ohmic losses. The structure of CL also determines parameters such as electron conductivity to the reaction sites. Since carbon particles conduct electrons, the carbon agglomerates in CL structure are also pathways for electrons to reach the reaction sites. The details of CL structure determine the effectiveness of this process (Lange *et al.*, 2012).

Finally, an important issue is that of water management (Wu and Djilali, 2012). The byproduct of elctrochemical reaction in CL is water. Under certain operating conditions including high relative humidity and/or current density, by product water condenses, and the presence of excess liquid water can result in the blockage or "flooding" of the oxidant/air pathways inside the porous structure of CL (Litster and Djilali, 2005; Schwarz and Djilali, 2007). Using the proper material, and engineering the pours structure of CL can help the water management issue in CLs.

The discussion above highlights a few of the reasons why controlling the structure of CL is vital for its performance. The CL fabrication process involved the preparation of a colloidal ink, its application and drying (see Appendix A), and as noted earlier, structures (agglomerates) that are formed during the ink preparation persist during the drying process (Kusano *et al.*, 2015). The relevant properties of the ink are therefore reviewed next.

1.2 Catalyst Layer Ink: A Colloidal Suspension

The catalyst layer ink is a colloidal suspension of carbon nanoparticles in an aqueous or alcohol solution (Sharma and Andersen, 2018). The main components are Pt/C particles, solvent (which can be water or a solution of water and some other dispersion media such as isopropyl alcohol), polymer ionomer solution (e.g. Nafion solution) and/or a hydrophobic agent (such as polytetrafluoroethylene (PTFE) or polyvinylidene fluoride (PVDF)). The presence of ionomer such as Nafion or a hydrophobic agent such as PTFE results in a *Hydrophilic* or *Hydrophobic* ink solution, respectively.

To make the CL, generally, a thin layer of prepared ink is dried until the excess water and solvent are evaporated. The dried ink forms the porous solid CL. There are different techniques to make the CL from the ink solution; for example one can brush the ink on a surface, use a doctor blade to form a uniform layer of the ink on a surface, or spray the prepared ink on a surface etc. Although each technique needs its own optimized ink solution formula, there are some common steps in ink preparation as follows: Pt/C particles are first wetted by distilled water and mixed with the required amount of solvent; the mixture is stirred for a few minutes using for example a magnetic stir bar or a high-shear mixer, followed by sonication for a longer time (e.g. half an hour) to control/reduce particle agglomeration; Nafion solution is then added to the mixture, and the procedure of mixing continues by sonication and/or stirring (for an hour or so). (Note that Nafion solution can be added to the Pt/C powder first, followed by adding the solvent (Park *et al.*, 2007).)

The final goal is to make a uniformly-distributed ink solution of Pt/C particles, water/solvent, and Nafion solution. A wide range of recipes and techniques are used by different groups to make catalyst layer inks (See Appendix A for more details). Despite years of research about this topic, there is still no agreement on the fundamental steps that can lead to a high performance catalyst layer. The main reason for this is the complexity of the processes and underlying phenomena.

Observing the agglomeration process of nanoparticles during ink preparation in the lab is a very challenging task. There are various techniques to observe nanoparticles, but they all have their limitations and challenges. For example, dynamic light scattering or DLS (Goldburg, 1999) devices are widely used in many works due to their relatively fast measurement times

and simple sample preparation. However, these measurements are volume-based (volume weighted), and the measurements are more sensitive to the presence of large particles which makes these devices suitable for specific samples (usually uni-modal with relatively narrow particle size distribution), and the interpretation of measurement is susceptible to input parameters (such as the refractive index of particles) and the complexity of the applied mathematical model for the light scattering/refraction. This makes these devices more appropriate for qualitative measurements, rather than detailed quantitative studies. Also, they usually require sample dilution, and despite the relatively simple sample preparation, the effect of dilution is not well understood for many samples (Shukla *et al.*, 2017). On the other hand, more sophisticated techniques such as electron microscopy (for example scanning electron microscope or SEM, and transmission electron microscopy or TEM) or neutron scattering (Shibayama *et al.*, 2014; Kusano *et al.*, 2015) are generally time consuming, preclude the presence of liquids, have complex sample preparation, are costly, and require complicated analysis.

These difficulties have limited the progress in further understanding of the ink preparation process. This is why most of the studies about ink preparation are based on a trial and error approach, yielding a wide range of recipes and techniques without sufficient understanding of why one formula works better than the other. The list of various recipes highlights the need for a deeper understanding of catalyst layer ink preparation.

1.3 Scope of Thesis

Given the challenges of experimentally studying the agglomeration process, recent improvements on computational capabilities can offer new paths to study this phenomenon.

In this work, we will develop further understanding of the fabrication process via state of the art modelling of colloidal inks. We perform simulations of agglomeration of particles under various conditions, and compare our simulation results to other analytical, numerical, and experimental studies to gain new insights about the CL ink. This will help us identify the mechanisms that impact the quality of the catalyst layer, and develop methods to control the final structure to reduce costs and/or achieve optimal performance and durability for specific applications. We believe this work can make significant contributions to fundamental knowledge as well as the commercial viability

of the next generation fuel cell technology.

The thesis is organized as follows: Chapter 2 discusses a number of the force fields and underlying models describing the interaction between particles in a colloidal suspension; Chapter 3 provides a detailed description of the mathematical model and numerical method used to simulate the dynamical multi-particle system representative of catalyst inks. The results of the simulations are presented in Chapter 4 together with a key aspect of this study: the application of network science concepts to analyze and interpret the simulation. The thesis closes with a summary of contributions, and avenues for further research.

Chapter 2

Physics of the Problem: Particle-Particle Interaction in the Catalyst Layer Ink

In a colloidal suspension of nanoparticles in a solvent medium, particles can interact through various forces such as van der Waals, electrostatic, and hydrophobic. Addition of polymer can also result in some other interactions such as depletion and steric repulsion. The importance of each force in a system depends on the type of particles and solvent, size of particles, presence of electrical charges in the system, shape of particles, and conformation of polymer molecules. For a better understanding of the physics of the problem, we review a number of the force fields and underlying models describing the interaction between particles in a colloidal suspension. This allows us to define a more relevant physical potential between particles in our simulations. The goal is to use this physical potential, instead of commonly used potential models such as Lennard-Jones, to provide a more realistic representation of the system in our simulations.

In the next step, we characterize these interactions for components in CL ink (for example, see Figure 2.1). The background related to catalyst inks was briefly reviewed in the preceding Chapter and is complemented by a more detailed discussion in Appendix A.

In this chapter, we discuss the most important interactions in a colloidal suspension of nanoparticles in a solvent medium.

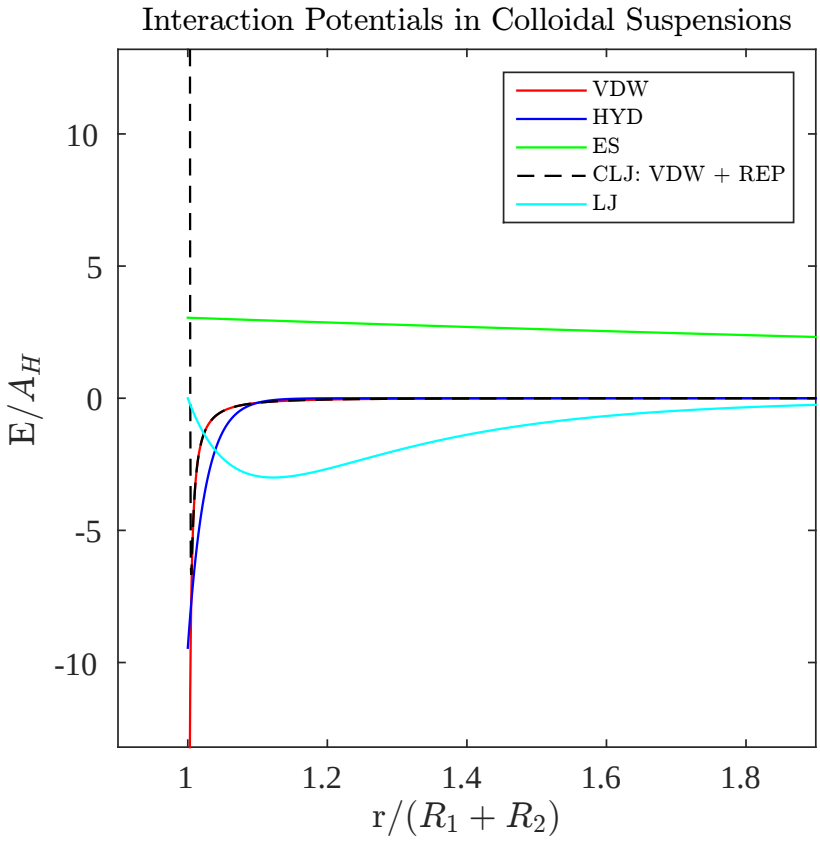

Figure 2.1: Examples of interaction potentials in a colloidal suspension between two spherical particles of radius R_1 and R_2. Corresponding relations are discussed throughout this chapter. Some typical values have been chosen for various parameters. VDW, HYD, ES, REP and LJ stand for van der Waals, hydrophobic, electrostatic, repulsive, and Lennard-Jones interaction potentials, respectively. E, A_H, and r are potential energy, Hamaker constant of carbon, and centre to centre distance between two spherical particles, respectively.

2.1 Van der Waals Interaction

The interaction between atoms can be divided into two types (Pauling, 1960; Drobny, 2011):

Chemical or covalent forces: These forces refer to interactions between atoms within a molecule, which cause interatomic bonding known as covalent or chemical bonds (also called bonded interactions). Covalent forces act over very short distances of the order of interatomic separations (0.1-0.2 nm), and are a result of complex quantum mechanical interactions.

Physical forces: These forces refer to interactions between unbounded discrete atoms and molecules, which result in physical bonds. Physical forces are responsible for holding together the atoms and molecules in solids and liquids, as well as in colloidal and biological assemblies. In contrast to chemical forces, physical forces are long-ranged.

One type of physical forces is the dipole-dipole interaction, which is the interaction between two polar molecules. The energy of dipole-dipole interaction can be written as (Stokes and Evans, 1996):

$$w(r,\theta_1,\theta_2,\phi) = -\frac{u_1 u_2}{4\pi\varepsilon_0\varepsilon r^3}[2\cos\theta_1\cos\theta_2 - \sin\theta_1\sin\theta_2\cos\phi] \tag{2.1}$$

where u_1 and u_2 are the dipole moments, ε_0 is the permittivity of free space, ε is the relative permittivity or dielectric constant of the medium, r is the separation, and two polar angles θ_1 and θ_2, and one azimuthal angle ϕ specify the orientation of the dipoles (see Figure 2.2). One can show that a Boltzmann averaging over all the orientations, results in an angle-averaged energy of (Israelachvili, 2010):

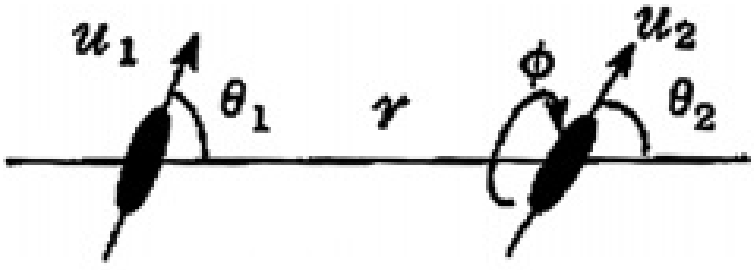

Figure 2.2: Dipole-dipole interaction. Reproduced from Israelachvili (2010).

$$w(r) = -\frac{{u_1}^2 {u_2}^2}{3(4\pi\varepsilon_0\varepsilon)^2 kTr^6} \qquad for \qquad kT > \frac{u_1 u_2}{4\pi\varepsilon_0\varepsilon r^3} \tag{2.2}$$

where k is the Boltzmann constant, and T is the temperature. The above Boltzmann-averaged interaction is known as the orientation or *Keesom* interaction.

Although not all molecules are polar, the dipole moment can be induced when a molecule or atom is present in an electric field. The polarizability of nonpolar atoms or molecules, α_0, is defined as (Bonin, 1997):

$$u_{ind} = \alpha_0 E \tag{2.3}$$

where u_{ind} is the induced dipole moment, and E is the electric field. The electric field can be an external field, or originate from a nearby molecule. Thus, the vicinity of a polar and a nonpolar molecules results in a dipole-induced dipole interaction with energy $w(r, \theta)$ of (Israelachvili, 2010):

$$w(r, \theta) = -u^2\alpha_0(1 + 3\cos^2(\theta))/2(4\pi\varepsilon_0\varepsilon)^2 r^6 \tag{2.4}$$

The effective interaction can be found by averaging over the angle θ, which results in (de Paula Peter Atkins, 2010):

$$w(r) = -u^2\alpha_0/(4\pi\varepsilon_0\varepsilon)^2 r^6 \tag{2.5}$$

Moreover, the polarization can also be induced in molecules with permanent dipole moment. Thus, the general relation for the net dipole-induced dipole energy for two molecules with permanent dipole moments of u_1 and u_2, and the polarizabilities of α_{01} and α_{02} can be written as:

$$w(r) = -\frac{[u_1^2\alpha_{02} + u_2^2\alpha_{01}]}{(4\pi\varepsilon_0\varepsilon)^2 r^6} \tag{2.6}$$

The above interaction energy is known as the *Debye* interaction or the induction interaction.

There is another important type of physical force between atoms or molecules which is called dispersion force. This force originates in quantum mechanics, and requires knowledge of quantum electrodynamics to be

fully understood. However, in simple words, it can be explained as follows: while the time average of the dipole moment of a nonpolar atom or molecule is zero, the instantaneous position of the electrons around protons can be considered as a temporary dipole at each instant. This instantaneous dipole can affect the nearby molecules, similarly to the permanent dipoles, and induce a dipole moment in them. The interaction between the two dipoles results in dispersion force. This force is very important because it is always present without depending on the properties of the molecules.

An expression for dispersion interaction energy between two atoms in a vacuum is (London, 1937):

$$w(r) = -\frac{3}{2}\frac{\alpha_{01}\alpha_{02}}{(4\pi\varepsilon_0\varepsilon)^2 r^6}\frac{h\nu_1\nu_2}{(\nu_1+\nu_2)} \tag{2.7}$$

where h is the Plank constant, and ν_1 and ν_2 are the orbiting frequency of electrons which correspond to the required energy to ionize the atom; the first ionization potential. The above equation is known as London equation, and the dispersion force is also called the London force.

So far, we introduced three important physical interactions which vary with the inverse sixth power of the distance: the induction force, the orientation force, and the dispersion force. These three distinct types of forces together are known as the van der Waals force. Thus, the corresponding relation for the van der Waals interaction energy between two dissimilar molecules can be written as:

$$\begin{aligned} w_{VDW}(r) &= -C_{VDW}/r^6 = -[C_{ind} + C_{orient} + C_{disp}]/r^6 \\ &= -[(u_1^2\alpha_{02} + u_2^2\alpha_{01}) + \frac{{u_1}^2{u_2}^2}{3kT} + \frac{3\alpha_{01}\alpha_{02}h\nu_1\nu_2}{2(\nu_1+\nu_2)}]/(4\pi\varepsilon_0)^2 r^6 \end{aligned} \tag{2.8}$$

One should note that the London theory of dispersion (and thus the above relation for van der Waals interaction) has some defects; for example it assumes only one single ionization potential for atoms and molecules, and also it cannot explain the interaction of molecules in a solvent. Thus, in 1963 McLachlan proposed a generalized theory of van der Waals which can also be used for interactions in a solvent. For two molecules or small particles 1 and 2 in a solvent medium 3, the McLachlan's expression (McLachlan, 1963a,b, 1965) for the van der Waals energy is as follows:

$$w_{VDW}(r) = -\frac{C_{VDW}}{r^6} = -\frac{6kT}{(4\pi\varepsilon_0)^2 r^6} \acute{\sum}_{n=0,1,2,\ldots}^{\infty} \frac{\alpha_1(i\nu_n)\alpha_2(i\nu_n)}{{\varepsilon_3}^2(i\nu_n)} \qquad (2.9)$$

where $\alpha_1(i\nu_n)$ and $\alpha_2(i\nu_n)$ are the polarizabilities of molecules 1 and 2, and $\varepsilon_3(i_n)$ is the dielectric permittivity of the medium 3, at imaginary frequencies $i\nu_n$, where

$$v_n = (\frac{2\pi kT}{h})n \approx 4 \times 10^{13} n \quad s^{-1} \qquad at \qquad 300K \qquad (2.10)$$

Note that the summation operator with a prime ($\acute{\sum}$) means that the zero frequency term (n=0) should be divided by 2.

2.1.1 Van der Waals Forces between Macroscopic Particles

The McLachlan's relation gives the van der Waals interaction energy between two molecules or small particles. However, to find the interaction between two macroscopic particles or surfaces, all the pair potentials between the atoms or molecules in each body should be summed. One can do this calculation for different geometries (for example between two spheres or two cylinders), and the final result for each particular geometry can be expressed in the following way: there are terms that include the properties of the geometry (such as radius, separation, etc.), and another term known as Hamaker constant which includes all the materials properties. Basically, everything except the geometry is included in the Hamaker constant. For example, for two macroscopic spheres of radii R_1 and R_2, and a surface to surface separation of D (see Figure 2.3), the van der Waals interaction energy is given by (Hamaker, 1937):

$$W_D = -\frac{A}{6}[\frac{2R_1R_2}{(2R_1+2R_2+D)D} + \frac{2R_1R_2}{(2R_1+D)(2R_2+D)} + \ln\frac{(2R_1+2R_2+D)D}{(2R_1+D)(2R_2+D)}] \qquad (2.11)$$

where A is the Hamaker constant.

A simple definition of Hamaker constant is (Butt *et al.*, 2006):

$$A = \pi^2 C \rho_1 \rho_2 \tag{2.12}$$

where C is the van der Waals coefficient in the atom-atom pair potential, and ρ_1 and ρ_2 are the number of atoms per unit volume in the two macroscopic bodies. This simple definition of Hamaker constant ignores the effect of neighbouring atoms. It assumes that the additivity holds which cannot be the case for condensed media (Nonadditivity means that the interaction between two particles is also affected by the presence of particles around them. For example, dispersion forces are nonadditive.). To avoid this issue, Lifshitz theory (Lifshitz, 1956) suggests the following expression for the Hakamer constant:

$$\begin{aligned} A = \pi^2 C \rho_1 \rho 2 &= \frac{6\pi^2 kT \rho_1 \rho_2}{(4\pi\varepsilon_0)^2} \acute{\sum}_{n=0,1,2,\ldots}^{\infty} \frac{\alpha_1(i\nu_n)\alpha_2(i\nu_n)}{{\varepsilon_3}^2(i\nu_n)} \\ &= \frac{3}{2} kT \acute{\sum}_{n=0,1,2,\ldots}^{\infty} [\frac{\varepsilon_1(i\nu_n) - \varepsilon_3(i\nu_n)}{\varepsilon_1(i\nu_n) + \varepsilon_3(i\nu_n)}][\frac{\varepsilon_2(i\nu_n) - \varepsilon_3(i\nu_n)}{\varepsilon_2(i\nu_n) + \varepsilon_3(i\nu_n)}] \end{aligned} \tag{2.13}$$

which can be approximated as:

$$A \approx \frac{3}{4} kT (\frac{\varepsilon_1 - \varepsilon_3}{\varepsilon_1 + \varepsilon_3})(\frac{\varepsilon_2 - \varepsilon_3}{\varepsilon_2 + \varepsilon_3}) + \frac{3h}{4\pi} \int_{\nu_1}^{\infty} (\frac{\varepsilon_1(i\nu_n) - \varepsilon_3(i\nu_n)}{\varepsilon_1(i\nu_n) + \varepsilon_3(i\nu_n)})(\frac{\varepsilon_2(i\nu_n) - \varepsilon_3(i\nu_n)}{\varepsilon_2(i\nu_n) + \varepsilon_3(i\nu_n)}) d\nu \tag{2.14}$$

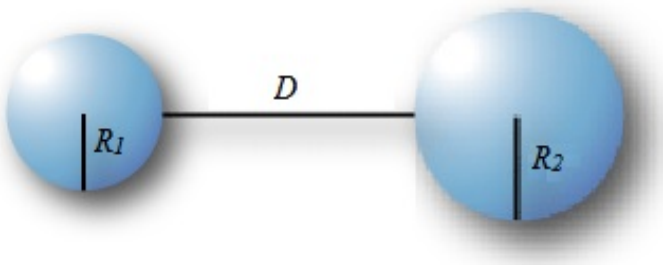

Figure 2.3: The interaction between two spherical particles.

where ε_1, ε_2, and ε_3 are the static (zero frequency) dielectric constants of the three media. Once the dependence of ε on ν is known (ε is usually given as a function of ν and refractive index, n) for particles and medium, Hamaker constant can be estimated using above relation. Note that rather than atomic scale parameters, Lifshitz theory uses the bulk properties, such as dielectric constant and refractive index, to estimate the Hamaker constant.

2.2 Electrostatic Interaction

The strongest physical force is the well-known inverse-square Coulomb force between two charged atoms or ions:

$$F_c(r) = \frac{Q_1 Q_2}{4\pi\varepsilon_0\varepsilon r^2} \tag{2.15}$$

where F_c is the Coulomb force, Q_1 and Q_2 are electric charges, r is the separation between charges, ε_0 is the permittivity of free space, and ε is the relative permittivity or dielectric constant of the medium. The corresponding energy for Coulomb interaction is:

$$w_c(r) = \frac{Q_1 Q_2}{4\pi\varepsilon_0\varepsilon r} \tag{2.16}$$

If the colloidal particles in solution are charged, they will interact electrostatically. However, the presence of ions in the solution results in the "screening effect" which can change the interaction dramatically. Screening effect in solutions is the reduction of electrostatic field of a charged particle due to the presence of mobile charge carriers. Each charged particle attracts opposite sign ions in the solution which reduces the electrostatic field away from the particle. The opposite sign ions can be either the counterions from the charged particles or the ions from electrolyte in the solution.

For two charged spheres with surface electrostatic potential of ψ_0 in a 1:1 electrolyte (which means both cation and anion of electrolyte have the same charge magnitude of 1), the electrostatic interaction can be approximated as:

$$W_{ES} = \left(\frac{R_1 R_2}{R_1 + R_2}\right)\frac{128\pi k_B T n_\infty}{\kappa^2}\tanh^2\left(\frac{e\psi_0}{4k_B T}\right)\exp(-\kappa D) \tag{2.17}$$

where R_1 and R_2 are the radius of spheres, k_B is the Boltzmann constant, T is the absolute temperature, n_∞ is the bulk electrolyte concentration, and κ is defined as:

$$\kappa = (\sum_i n_{\infty i} e^2 z_i^2 / \varepsilon_0 \varepsilon k_B T)^{(1/2)} \tag{2.18}$$

where $n_{\infty i}$ is the ionic concentration of ions i in the bulk or reservoir of solution, and z_i is the charge magnitude of ions i (which is 1 for the case of 1:1 electrolyte). κ^{-1}, known as Debye length, is the characteristic length or thickness which mobile charge carriers screen out the electric field of charged particles.

For cases more complicated than 1:2, 2:1, and z:z electrolytes, numerical calculations are required in order to find an accurate interaction potential between charged particles (e.g. Grahame, 1953). However, there are models which can give useful approximate analytical expressions for interaction potential for particular cases.

An interesting case is the interaction of charged particles in a solution that contains both polyelectrolyte and electrolyte. Polyelectrolytes get ionized to charged polyelectrolyte macroions that are very large in size, and corresponding counterions which can be very high in numbers. When the particles in solution are in close proximity to each other, the polyelectrolyte macroions are forced out from the gap between the particles at small enough separations, and the screening effect happens by the electrolyte ions and polyelectrolyte counterions. A relation for the interaction force between two spheres in a solution of a 1:1 salt electrolyte and polyelectrolyte counterions of charge 1 is given by Tadmor *et al.* (2002) as:

$$F_{ES} = (\frac{R_1 R_2}{R_1 + R_2}) \frac{128 \pi k_B T n_{eff}}{\kappa_{eff}} \tanh^2(\frac{e\psi_0}{4 k_B T}) \exp(-\kappa_{eff} D) \tag{2.19}$$

which results in an interaction potential of:

$$W_{ES} = (\frac{R_1 R_2}{R_1 + R_2}) \frac{128 \pi k_B T n_{eff}}{\kappa_{eff}^2} \tanh^2(\frac{e\psi_0}{4 k_B T}) \exp(-\kappa_{eff} D) \tag{2.20}$$

where again R_1 and R_2 are the radii of spherical particles, k_B is the Boltzmann constant, T is the absolute temperature, and ψ_0 is the potential at the

surface. n_{eff} is the effective salt concentration inside the gap and is defined as:

$$n_{eff} = \sqrt{n_s n_c} \tag{2.21}$$

where n_s is the bulk ion concentration of the monovalent anions (the concentration in the buffer solution), and n_c is the bulk ion concentration of the monovalent cations:

$$n_c = n_s + Z n_p \tag{2.22}$$

where n_p is the bulk concentration of the macroions (or polymer concentration), Z is the number of elementary charges per polyelectrolyte chain, and κ_{eff} is defined as:

$$\kappa_{eff} = [\varepsilon_0 \varepsilon k_B T / 2 n_{eff} e^2]^{-1/2} \tag{2.23}$$

Also, another useful equation is the relation between surface charge density, σ, and the surface potential, ψ_0, which is given as:

$$\sigma = \sqrt{8 \varepsilon \varepsilon_0 k_B T} \sinh(e\psi_0 / 2 k_B T) [n_s (n_s + Z n_p)]^{1/4} \tag{2.24}$$

When the surface charge density is known, surface potential can be found from the above relation which later on can be used in the interaction potential relation between two particles (Equation 2.20).

2.3 Depletion Interaction

Presence of smaller particles (such as polymers or small colloidal particles) in colloidal suspension of larger particles results in a force known as depletion force. As two large particles approach, the concentration of smaller particles (known as depletants) in the gap region between large particles changes. The variation of depletants concentration in the gap region changes the osmotic pressure in this region compared to the outside the gap which contains the bulk concentration of depletants. The difference between osmotic pressure of inside and outside the gap results in depletion force. This interaction was

first introduced by Asakura and Oosawa (1954) to explain the destabilization or flocculation of colloidal suspensions.

For uncharged depletants, the depletion potential between two spherical particles is given by Mao *et al.* (1995) as:

$$\frac{W_{Dep}}{k_B T} = 0 \qquad \text{for } h > 2\sigma \tag{2.25}$$

$$\frac{W_{Dep}}{k_B T} = (\frac{2R_1R_2}{R_1+R_2})\frac{\phi^2}{5\sigma}(12-45\lambda+60\lambda^2-30\lambda^3+3\lambda^5) \qquad \text{for } 2\sigma > h > \sigma \tag{2.26}$$

$$\frac{W_{Dep}}{k_B T} = (\frac{2R_1R_2}{R_1+R_2})(-\frac{3\phi}{\sigma}\lambda^2+\frac{\phi^2}{5\sigma}(12-45\lambda-60\lambda^2)) \qquad \text{for } h < \sigma \tag{2.27}$$

where R_1 and R_2 are the radius of spherical particles, σ is the diameter of depletants, h is the minimum separation distance between particle surfaces, ϕ is the volume fraction of depletants, and $\lambda = (h-\sigma)/\sigma$.

The above equations represent the depletion force to the second order in ϕ. As can be seen from the equations, there is a positive maximum value of $W_{Dep}/k_BT = 12R\phi^2/5\sigma$ at $h_{max} = \sigma(1-\frac{3}{2}\phi)$, which suggest a depletion repulsion force at separations larger than h_{max}. However, at closer separations, the force switches sign and a stronger attractive depletion force appears. This attractive depletion force is responsible for the flocculation of some colloidal suspensions.

When the depletant particles are charged, both magnitude and range of depletion force increases (e.g. Asakura and Oosawa, 1954, 1958; Walz and Sharma, 1994). However, due to the complexity of the problem, a numerical solution is required to obtain the depletion force (e.g. Walz and Sharma, 1994). On the other hand, the presence of low molecular salts in the solution besides the larger charged depletants reduces the depletion force rapidly.

2.4 Hydrophobic Interaction

The real origin of hydrophobic force is still a mystery. Hydrophobic (meaning "water fearing") interaction is an attractive interaction between hydrophobic surfaces in water which results in the agglomeration of these hydrophobic

substances. While the understanding of this force has been the subject of many works for the past few decades, it was experimentally measured by Israelachvili and Pashley (1982) for the first time. Different scenarios have been proposed to explain hydrophobic interaction (e.g. Israelachvili and Pashley, 1984; Christenson and Claesson, 1988; Claesson and Christenson, 1988; Attard, 1989; Podgornik, 1989; Craig *et al.*, 1993; Parker *et al.*, 1994; Pratt and Chandler, 1977; Tyrrell and Attard, 2001). One explanation is that this interaction can be due to the reduction of freedom of water molecules to form the preferred hydrogen bonding network around the hydrophobic surface (Donaldson Jr *et al.*, 2014). Water molecules cannot form hydrogen bonds with hydrophobic surfaces, and the presence of a hydrophobic surface in water disrupts the hydrogen bonded network of water molecules. The rearrangement of water molecules near hydrophobic surfaces is entropically unfavorable (e.g. Meyer *et al.*, 2006), thus hydrophobic surfaces prefer to associate with each other to reduce this effect.

Despite many unanswered questions regarding fundamental understanding of the hydrophobic interactions, Donaldson Jr *et al.* (2014) have recently suggested a general potential interaction which can describe the existing experimental measurements data. The general interaction potential per unit area between two surfaces is as follows:

$$W_{Hyd} = -2\gamma_i(Hy)\exp(-D/D_H) \tag{2.28}$$

where D is the separation distance between two hydrophobic surface, γ_i is the hydrophobic-water interfacial tension, and $D_H \approx 0.3-2$ nm is the decay length that depends on the precise system and conditions. Hy is the Hydra parameter and is defined as $Hy = 1 - a_0/a$, where a_0 is the hydrophilic area and a is the hydrophobic area at a given interface. Thus, $Hy = 1$ defines the maximum hydrophobic interaction, while $0 < Hy < 1$ corresponds to a partially hydrophobic surface.

Also, using Derjaguin approximation (Derjaguin, 1934), the hydrophobic interaction between two spheres with radii R_1 and R_2 can be given as:

$$W_{Hyd} = -\pi(\frac{2R_1R_2}{R_1+R_2})2\gamma_i(Hy)D_H\exp(-D/D_H) \tag{2.29}$$

2.5 Steric Repulsive Interaction

When two atoms are brought very close to each other, their electron clouds overlap which results in a strong repulsive force. This repulsive force has very short range and increases rapidly as the separation decreases. This force, which is a result of the finite size of atoms, can be modelled in different ways such as hard sphere or power-law potential.

For hard sphere potential, it is assumed that the particles are rigid and impenetrable. This potential can be modelled as:

$$W_{HS} = +(\sigma/r)^n \qquad \text{where } n \longrightarrow \infty \tag{2.30}$$

or equivalently

$$W_{HS} = \begin{cases} 0 & \text{if } r > \sigma \\ \infty & \text{if } r < \sigma \end{cases} \tag{2.31}$$

where σ is the diameter of particles and r is the centre-to-centre distance.

For power-law potential, we have:

$$W_{PL} = +(\sigma/r)^n \tag{2.32}$$

where now, n is an integer number. The power-law repulsive potential is used as the repulsive term in different interaction potentials such as the well known Lennard-Jones (LJ) potential:

$$W_{LJ}(r) = \frac{C_{12}}{r^{12}} - \frac{C_6}{r^6} = 4\epsilon[(\frac{\sigma}{r})^{12} - (\frac{\sigma}{r})^6] \tag{2.33}$$

where ϵ and σ are the LJ potential parameters to be determined for each case (Figure 2.4). The LJ potential was proposed as the total interaction potential between atoms and small molecules. It has an inverse sixth-power attractive term (same as the van der Waals interaction), and an inverse 12 exponent repulsive term. While the attractive term originates in quantum theory, the inverse 12 exponent was chosen for mathematical convenience (any number within 14 ± 5 provides good agreement with experimental data (Israelachvili, 2010)).

For interaction between macroscopic colloid particles, one can integrate the LJ potential over the volume of the particles to find a potential known as the colloid Lennard-Jones (CLJ). CLJ potential has an attractive term which is the same as the van der Waals interaction between macroscopic particles, and a repulsive term which is given by Henderson *et al.* (1997) as:

$$W_{12}(r) = C_{12}(\frac{16}{4725}\pi^2 a^3 b^3)\frac{\sum_{n=0}^{8} P_{16-2n}(a,b)r^{2n}}{([(r+a)^2-b^2][(r-a)^2-b^2])^7} \tag{2.34}$$

where C_{12} is the interaction parameter between two molecules in LJ potential, a and b are the radii of colloidal particles, and r is the centre-to-centre separation between two particles. The polynomials $P_m(a,b)$ are given as:

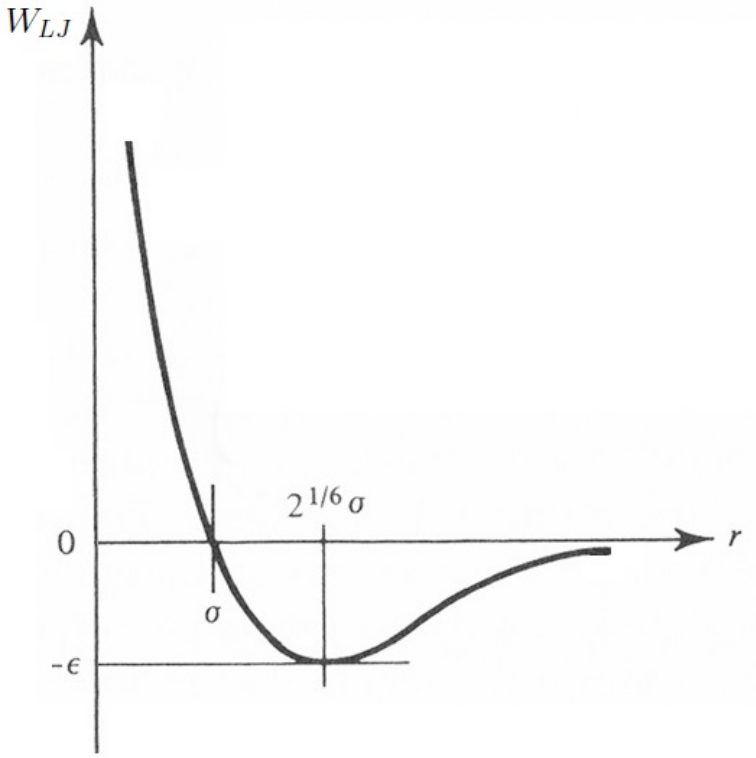

Figure 2.4: Lennard-Jones potential.

$$P_0(a,b) = 525 \tag{2.35}$$

$$P_2(a,b) = -420(a^2 + b^2) \tag{2.36}$$

$$P_4(a,b) = -168(25a^4 - 77a^2b^2 + 25b^4) \tag{2.37}$$

$$P_6(a,b) = 28(a^2 + b^2)(325a^4 - 838a^2b^2 + 325b^4) \tag{2.38}$$

$$P_8(a,b) = -2(2275a^8 + 13552a^6b^2 - 38502a^4b^4 + 13552a^2b^6 + 2275b^8) \tag{2.39}$$

$$P_{10}(a,b) = -4(a^2 + b^2)(875a^8 - 11844a^6b^2 + 22898a^4b^4 - 11844a^2b^6 + 875b^8) \tag{2.40}$$

$$P_{12}(a,b) = 56(a^2 - b^2)^2(70a^8 - 49a^6b^2 - 762a^4b^4 - 49a^2b^6 + 70b^8) \tag{2.41}$$

$$P_{14}(a,b) = -700(a^2 - b^2)^4(a^6 + 11a^4b^2 + 11a^2b^4 + b^6) \tag{2.42}$$

$$P_{16}(a,b) = -35(a^2 - b^2)^6(5a^4 + 14a^2b^2 + 5b^4) \tag{2.43}$$

Beside the above mentioned steric repulsive force which prevents penetration of particles into each other, there is another steric repulsive force known as polymer-mediated steric force which plays an important role in colloidal suspensions. The presence of polymers in a solution can result in stabilization of the colloidal particles. When the separation between two polymer-covered surfaces becomes less than twice the thickness of the adsorbed layer, the polymer chains between surfaces start to compress. This is entropically unfavorable which results in a repulsive force.

The polymer mediated steric interactions are generally very complex. One of the factors defining the interaction is the conformation of polymer on the surface. For two brush-bearing spherical particles, the steric repulsion potential is given by Likos *et al.* (2000) as:

$$\frac{W_{St}}{k_B T} = \begin{cases} \infty & r < 2R_C \\ f(y) & 2R_C < r < 2(R_C + L) \\ 0 & 2(R_C + L) < r \end{cases} \tag{2.44}$$

where $y = (r - 2R_C)/(2L)$, and

$$f(y) = \frac{16\pi R_C L^2}{35 s^3}[28(y^{-1/4} - 1) + \frac{20}{11}(1 - y^{11/4}) + 12(y - 1)] \tag{2.45}$$

In the above equations, R_C is the radius of particles, L is the thickness of the brush layer, r is the centre-to-centre distance, and s is the mean distance between two polymeric molecules on the surface.

Chapter 3

Numerical Tools

One candidate for simulating a colloidal suspension is a CFD (Computational Fluid Dynamics) code that also resolves particles. Using a CFD code, the solvent and all the corresponding effects of particles' movements in the system can be investigated. However, resolving the formation of large scale structures requires high number of particles in the simulation. Moreover, to compare the simulation results with real structures, it is required to run simulations in 3D. We have realized that it becomes computationally very expensive to use a CFD code to simulate a 3D colloidal suspension with a high number of particles. Because of this issue, we use an N-body code to simulate the agglomeration of particles.

3.1 What is an N-body Code?

In general, N-body codes are designed to simulate a dynamical system of particles that interact with each other under the influence of various forces. Classically, an "N-body problem" was referred to the prediction of celestial bodies motion, and N-body codes were developed to solve these problems. However, nowadays, a wide spectrum of problems, ranging from astrophysical objects to individual atoms in a gas cloud, can be simulated using N-body simulations.

Fundamentally, in an N-body simulation, the motion of particles is described by Newton's law. For an i-th particle in the system, we have:

$$\vec{F_i} = m_i \vec{a_i} = m_i \frac{d\vec{v_i}}{dt} = m_i \frac{d^2 \vec{r_i}}{dt^2} \tag{3.1}$$

where $\vec{F_i}$ is the corresponding total force on i-th particle, m_i is its mass, $\vec{a_i}$ its acceleration, $\vec{v_i}$ its velocity, $\vec{r_i}$ its position, and t is time. The total force on i-th particle in the system is:

$$\vec{F_i} = \sum_{j \neq i} \vec{F_{ij}} \tag{3.2}$$

where $\vec{F_{ij}}$ is the force on the i-th particle due to the j-th particle. The goal in an N-body simulation is to find the coordinates and velocities of particles in the system at $t = t_f$ if the initial coordinates and velocities at $t = t_0$ are given. Since the dynamical behavior of particles in colloidal suspensions of interest can be described by Newton laws, an N-body code is a suitable tool to study these systems.

One should note that a shortcoming of this numerical method is that the solvent is not explicitly accounted for in our system. Generally, the problem of hydrodynamic interactions in a system with high number of particles is difficult to solve due to the long range nature of the phenomenon. Direct numerical simulation techniques that solve Navier-Stokes equations combined with motion equations of particles are computationally very expensive (Peng *et al.*, 2010; Choi and Djilali, 2016), and thus a limited number of particles can be considered in each simulation. However, hydrodynamic interactions associated with the presence of a solvent can also be approximately accounted for. There are many studies that use Stokes' drag law to model the hydrodynamic interaction (Higashitani and Iimura, 1998; Becker *et al.*, 2009; Becker and Briesen, 2010; Peng *et al.*, 2010; Eggersdorfer *et al.*, 2010). They assume a free draining approximation which means each particle is treated as there is no other particle in the system to disturb the flow field. We consider a similar approach to approximately model the hydrodynamic interactions in our N-body simulations (see section 4.7).

On the other hand, using an N-body code allows us to consider high number of particles in our simulations, so we can study the formation of structures at different scales.

Thus, altogether, considering the systems (colloidal suspensions) of our interest, the available computational power, and the need for simulating sys-

tems in 3D with high number of particles, an N-body code has been chosen to simulate our colloidal suspensions.

3.2 REBOUND: An N-body Code

For this project, we have used an N-body code called REBOUND (Rein, H. and Liu, S.-F., 2012; Rein and Tamayo, 2015; Rein and Spiegel, 2015). It is an open-source, multi-purpose, and highly modular N-body code, and can be customized to work on a variety of problems.

One of the most important features of REBOUND for us is the fact that it is one of the only publicly available N-body codes that can also detect collisions between particles. This makes it useful to simulate a colloidal suspension system. This feature is important for this project because first of all, we consider realistic physical forces in our simulations rather than commonly used potential models, thus, the repulsive term in potential models (which prevents particles from coming into contact with each other) is ignored. In other words, we define systems where the interaction between particles may only be attractive. When no repulsive interaction between particles is considered, the ability of defining rigid particles (which means the steric repulsive force due to finite size of particles is already included) that can collide with each other is a key asset. Also, to analyze the results of our simulations, we will use concepts from network science, and to do so, we need to determine all the particles in contact (see ***Chapter 4*** for more details). So, again, detecting collision is an important feature for this work.

Figure 3.1 shows a typical example of a REBOUND simulation where an attractive interaction force has been defined between particles as well as a velocity dependent drag force. After enough time is passed, particles lose energy and agglomerate to form various agglomeration patterns.

REBOUND is an N-body integrator, i.e. it integrates the motion of particles in a system interacting via some forces. Several different symplectic integrators (such as WHFast, SEI, LEAPFROG) and a high accuracy non-symplectic integrator with adaptive timestepping (IAS15) are implemented in REBOUND (Rein, H. and Liu, S.-F., 2012; Rein and Tamayo, 2015; Rein and Spiegel, 2015). It is also parallelized to reduce computational time for large simulations. The code is written entirely in C and can be called from C or Python.

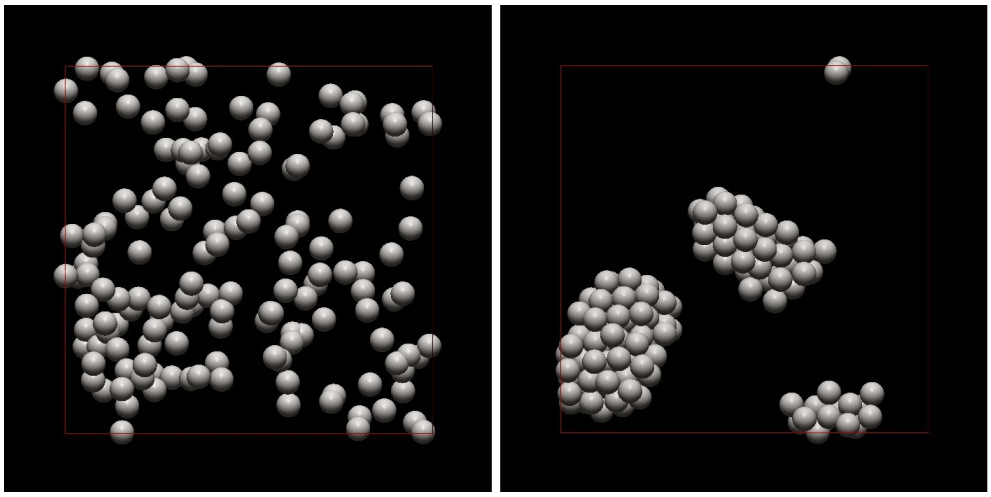

Figure 3.1: Example of the snapshots of a simulation in REBOUND. Left: Particles distributed in a box. Right: Agglomeration of particles.

Although N-body codes are more popular in the field of astrophysics, the REBOUND can be readily applied to problems in other fields such as molecular dynamics or granular flows (Rein, H. and Liu, S.-F., 2012) and several examples are given in the REBOUND package.

To be able to run simulations of interest, we have made some changes to the code. As has been mentioned, N-body codes are widely used in the field of astrophysics where interaction between particles is governed by gravitational force. In the REBOUND, each particle is defined by parameters such as mass, radius, position, velocity, and acceleration. To increase force options, we have modified the code by adding more parameters (similar to mass) to the particles definition. Now, we can define various group of particles in one simulation with different interaction potentials between them. For example, this is useful when only a portion of particles in the system are charged and interact via electrostatic interaction. We also have introduced a velocity dependent drag force to resemble the effect of solvent friction in real systems (see section 4.7 for more details).

3.3 Numerical Schemes in REBOUND

When solving a problem numerically, various numerical techniques can be used based on the nature of equations to be solved. "Symplectic integrators" are integration schemes designed for the numerical solutions of Hamiltonian systems; i.e. systems whose dynamics can be described by Hamilton's equations. When a Hamiltonian is not explicitly time dependent, it represents a constant of motion that is equal to the total energy of the system. In Hamiltonian mechanics, the state of the system is described by a set of canonical coordinates $(\boldsymbol{q},\boldsymbol{p})$, where $\boldsymbol{q}$ and $\boldsymbol{p}$ represent position and momentum, respectively. The evolution equation is given by:

$$\frac{d\boldsymbol{p}}{dt} = -\frac{\partial \boldsymbol{H(q,p)}}{\partial \boldsymbol{q}} \tag{3.3}$$

$$\frac{d\boldsymbol{q}}{dt} = \frac{\partial \boldsymbol{H(q,p)}}{\partial \boldsymbol{p}} \tag{3.4}$$

where $\boldsymbol{H(q,p)}$ is the Hamiltonian which corresponds to the sum of kinetic and potential energy in the system (i.e. the total energy) for a closed system. The time evolution of the Hamiltonian conserves the symplectic two-form $d\boldsymbol{p} \wedge d\boldsymbol{q}$ (i.e. it preserve the infinitesimal phase-space volume), and the numerical scheme that conserves this two-fold is also called symplectic (Yoshida, 1992). Symplectic integrators are particularly well suited to physical problems involving multi-body dynamics and are implemented in many of the simulation codes, including REBOUND.

All symplectic integrators in REBOUND follow the Drift-Kick-Drift (DKD) scheme, but three sub-steps are implemented differently. Below, we explain the details of the integrator used in our simulations (Leapfrog) in details, and introduce some of the other ones briefly.

Leapfrog: Leapfrog is a symplectic, time reversible and second order accurate integrator (i.e. the error after a single time step is at $O(\Delta t^3)$ where Δt is the timestep). The Drift-Kick-Drift scheme for this integrator is implemented as follows:
Assume the position and velocity of the particles are known at the beginning

of a time-step, $\boldsymbol{r}^n$ and $\boldsymbol{v}^n$. The goal is to find the positions and velocities after one time step, $\boldsymbol{r}^{n+1}$ and $\boldsymbol{v}^{n+1}$. Under a Drift-Kick-Drift scheme:

$$\boldsymbol{r}^{n+\frac{1}{2}} = \boldsymbol{r}^n + \boldsymbol{v}^n \frac{\Delta t}{2} \qquad \text{(Drift)} \tag{3.5}$$

$$\boldsymbol{v}^{n+1} = \boldsymbol{v}^n + \boldsymbol{a}^{n+\frac{1}{2}} \Delta t \qquad \text{(Kick)} \tag{3.6}$$

$$\boldsymbol{r}^{n+1} = \boldsymbol{r}^{n+\frac{1}{2}} + \boldsymbol{v}^{n+1} \frac{\Delta t}{2} \qquad \text{(Drift)} \tag{3.7}$$

where Δt is the timestep, and $\boldsymbol{a}$ represents the acceleration (calculated from the interaction force/potential). Thus, each sub-step in this Drift-Kick-Drift scheme is a simple Euler step, where first the position is evolved for half timestep while the velocity is fixed; then the velocity is evolved for a full timestep while the position is fixed, and at the end, the position is evolved for another half timestep. Another way of presenting this is by considering the Hamintonian operator. For a system where the total energy can be described by a Hamiltonian consisting of a kinetic term plus a potential term, we have:

$$\boldsymbol{H(q,p)} \ = \boldsymbol{H}_{Kinetic}(\boldsymbol{p}) + \boldsymbol{H}_{Potential}(\boldsymbol{q}) \tag{3.8}$$

where the Drift step is evolved under the kinetic term and the Kick step is evolved under the potential term. Thus, if the evolution operator of the system during one timestep under the Hamiltonian is $\hat{H}(\Delta t)$, then the following operator represents a single timestep in the Leapfrog DKD scheme:

$$\hat{H}_{Kinetic}(\frac{\Delta t}{2}) \hat{H}_{Potential}(\Delta t) \hat{H}_{Kinetic}(\frac{\Delta t}{2})$$

A similar scheme of Kick-Drift-Kick can also be applied, but a slightly better performance for REBOUND was reported by Rein, H. and Liu, S.-F. (2012) using a Drift-Kick-Drift scheme.

One should note that while the symplectic behavior of Leapfrog integrator can be useful for particular problems discussed above, if the corresponding conditions are not satisfied the integrator loses some of its desirable features.

For example, if velocity dependent forces are introduced (or self gravity or approximation for collisions are considered), the integrator will no longer be symplectic or time reversible, and it will only be first order accurate (i.e. the error after a single time step is at $O(\Delta t^2)$) rather than second order (Rein and Tremaine, 2011).

Although we introduce a velocity dependent drag force in our simulations, a small enough timestep for Leapfrog will produce sufficiently accurate results for the purpose of this study. Thus, since other available integrators in REBOUND are computationally more expensive, we decided to used Leapfrog considering our computational resources.

Wisdom-Holman Scheme: In this scheme proposed by Wisdom and Holman (1991), the Hamiltonian of the system is broken into two parts; a *"Keplerian"* part which represents the motion of bodies with respect to the central body, and an *"Interaction"* part which represents the perturbations of the bodies on each other. When this type of splitting the Hamiltonian is considered, the symplectic integrator is known as a "mixed-variable symplectic integrator". This scheme is best suited for systems where there is a predominant Keplerian motion around a body, and the interactions between other bodies can be considered as perturbations to this predominant motion. A good example of this can be the motion of planets around a star similar to our solar system. If we divide the Hamiltonian to a Keplerian part , $\boldsymbol{H}_{Keplerian}$, and an interaction part, $\boldsymbol{H}_{Intercation}$, the evolution of system during each timestep follows a second order Leapfrog manner that can be described by corresponding Hamiltonian operators as:

$$\hat{H}_{Keplerian}(\frac{\Delta t}{2})\hat{H}_{Interaction}(\Delta t)\hat{H}_{Keplerian}(\frac{\Delta t}{2})$$

In REBOUND the Wisdom-Holman scheme has been implemented and improved to introduce more accurate and faster integrators such as WHFast (Rein and Tamayo, 2015). One should note that while Wisdom-Holman integrators can be very accurate for long term integrations of particular systems, they are computationally more expensive than Leapfrog integrator since an iterative approach is used to solve the Kepler's equation for each particle during each timestep.

Symplectic Epicycle Integrator (SEI): Similar to Wisdom-Holman integrators, symplectic epicycle integrator is a mixed variable symplectic scheme

for the sheering sheet (Rein and Tremaine, 2011). It is a second order and time reversible integrator.

IAS15: Integrator with Adaptive Step-size control, 15th order (or IAS15) is a very high order, non-symplectic integrator. While many symplectic integrators have been developed especially for long term integrations, there are some problems using these integrators. First of all, they are better suited for Hamiltonian systems. When dissipation or non-conservative forces are introduced in the system, the symplectic nature of the problem is lost. Also, it becomes very difficult to keep the symplecticity of these integrators while having an adaptive timestep.

When very high accuracy in integrations is required, it has been reported that non-symplectic integrators can be as good as and as fast as or faster than symplectic integrators (Rein and Spiegel, 2015). However, for problems where only qualitative behavior of the system is of interest and low to medium accuracy is sufficient, symplectic integrators have the advantage that a larger timestep can be chosen. Thus, considering the problem to be studied, a proper integrator should be considered.

IAS15 in REBOUND is built based on Gauss-Radau integration scheme suggested by Everhart (1985). It can handle both conservative and non-conservative forces, and can integrate variational equations. For most cases, the accuracy can be kept down to machine precision.

In this work, we run our simulations on a supercomputer cluster. While most of the features in REBOUND are parallelized with both OpenMP (Open Multi-Processing) and MPI (Message Passing Interface), IAS15 was not available for MPI at the time this work was being conducted, so, this integrator could not be used for our work to run simulations on a cluster.

3.4 Simulations Characteristics

One technical difficulty to use real physical potentials in codes that capture collision between particles is the stability of simulation when particles are very close or in contact with each other. For example, we typically consider spherical carbon nanoparticles of 20 nm radius. The van der Waals force between two carbon nanoparticles increases dramatically as two particles get very close to each other, at distances less than 0.01 of particles radii (see Figure 2.1). So, either smaller timestep is required for a stable simulation

which makes simulations much longer and computationally much more expensive, or someone can cut the potentials at very small distances while still capturing the main features of the force. We consider a combination of these techniques. Thus, based on our computational resources, we decrease the timesteps as much as possible, and we also cut the potential at very close distances to help the stability of the simulation.
For example, when the actual size of particles is 1 unit, we define the interaction potential in our simulations based on this actual size but we choose the size of particles in the simulation to be slightly larger than 1 (for example 1.01). This way, particles do not experience extremely large forces when they are in contact, which helps the stability of the simulation. Studies that use potential models such as Lennard-Jones potential do not face this problem since the repulsive term in those potential models become dominant as the separation between particles decreases. However, capturing the collision between particles and forming structures where particles are really in contact and touch each other is vital for the network analysis we do, so we had to overcome this difficulty using above mentioned techniques.

In a typical simulation, we consider 1000 spherical particles. In dimensionless units, the radius of a particles is around 1 unit, and the size of simulation volume is $100 \times 100 \times 100$. We change the size of simulation volume to change the volume concentration of particles. For each simulation, all particles are distributed randomly within the simulation volume. We also consider a periodic boundary condition in our simulations.

For each desired case, all other relevant parameters, such as ones to determine the interaction force, are defined based on that specific case. For example, in a simulation of carbon nanoparticles that are interacting via van der Waals force, the interaction potential between particles is defined as (see section 2.1.1 for more details) :

$$W_D = -\frac{A}{6}\Big[\frac{2R_1R_2}{(2R_1+2R_2+D)D} + \frac{2R_1R_2}{(2R_1+D)(2R_2+D)} + \ln\frac{(2R_1+2R_2+D)D}{(2R_1+D)(2R_2+D)}\Big] \quad (3.9)$$

where R_1 and R_2 are the radii of two spherical particles (which are equal in this study, $R_1 = R_2 = R$), D is the surface to surface separation, and A is the Hamaker constant. The typical numbers that we use to define our system

are as follows:

Particle radius $= 20 \times 10^{-9}\ m$

Density of carbon $= 2000\ kg/m^3$ (so the mass can be calculated to find the acceleration)

Carbon-Carbon Hamaker constant $= 3.03 \times 10^{-19}\ J$

Typical simulation time step $= 5 \times 10^{-11}\ s$

which in our dimensionless system are converted to (all other parameters are scaled to become dimensionless as well):

Particle radius $= 1$

Carbon-Carbon Hamaker constant $= 1$

Typical simulation time step $= 5 \times 10^{-11}$

For simulations with the hydrophobic force as the interaction between particles, the interaction potential is defined as:

$$W_{Hyd} = -\pi(\frac{2R_1R_2}{R_1+R_2})2\gamma_i(Hy)D_H \exp(-D/D_H) \tag{3.10}$$

where D is the separation distance between two hydrophobic surface, γ_i is the hydrophobic-water interfacial tension, and D_H is the decay length, and Hy is the Hydra parameter (see section 2.4 for details). R_1 and R_2 are the radii of two spherical particles which are equal in this study, $R_1 = R_2 = R$. The typical numbers for simulations with the hydrophobic interaction between particles are as follows:

Particle radius $= 20 \times 10^{-9}\ m$

$D_H = 1 \times 10^{-9}\ m$ (A typical decay length)

$\gamma_i = 22.8 \times 10^{-3}\ J/m^2$ (Hydrophobic-water interfacial tension)

$Hy = 1$ (Hydra parameter)

Since van der Waals and hydrophobic forces are the dominant attractive forces in a system similar to colloidal suspensions of interest, most of the simulation results presented in this work consider one of these forces as the interaction between particles.

Chapter 4

Results

4.1 Data Analysis

To study a structure that is formed from smaller components, one needs to find a way to define or characterize the structure.

Proper characterization of the system is the key for studying the state of the system. There are many problems that involve a system of particles, and understanding related phenomena requires well defined parameters that can be determined at different stages of the process. A good example of this is the behavior of a group of atoms. With only a few in the system, problems at microscopic level can be investigated, while the bulk behavior (macroscopic level) requires considerations of many atoms interactions. At two extreme levels (microscopic and macroscopic), the systems can be studied carefully with different sets of parameters that describe the system. However, for systems between microscopic and macroscopic levels (i.e. mesoscale), a main challenge remain to define a set of quantities/parameters/concepts which can describe the system, and are also translatable/applicable to both sides of the spectrum. An example of this problem is understanding the transition of liquid (or liquid-like) state to solid (or solid-like) state in systems at microscopic, intermediate or macroscopic scales (i.e. with different number of atoms) which requires defining new concepts that are valid at different scales (Adams and Stratt, 1990).

Depending on the problem, systems can be described in various ways. For example in an ordered structure such as a crystal, atoms are positioned in a periodic arrangement. There is a repeating pattern that defines the entire

crystal lattice, and the smallest group of particles that shows this pattern is called "unit cell". The geometry of this unit cell can be described by the length of cell edges and the angles between them. The atomic arrangement in a crystal can be studied using different techniques such as X-ray diffraction, and it is the topic of the crystallography science.

An agglomeration in a colloidal suspension is also a structure formed from smaller individual colloidal particles. To understand how various conditions can result in different agglomeration patterns, we need to define or characterize these agglomerations.

In the systems that we are interested in (i.e. colloidal suspensions similar to catalyst layer ink), the individual components are nanoscale colloidal particles (in our case, spherical carbon nanoparticles of 20 nm size in radius). Because of the corresponding size and scale in these systems, the interaction force profiles between these colloidal particles are different than those between atoms or molecules in crystals. Thus, they usually form structures that are not very well ordered (like crystals), but they are not completely random either, and various patterns can be characterized using different parameters.

For example, a group of parameters usually used to characterize agglomerations structures are length related quantities such as max/mean/min size, area, aspect ratio (the maximum ratio of the width to the height of a structure), and other quantities that define the shape, elongation or sphericity of the structure (Podczeck and Mia, 1996; Riley *et al.*, 2003; Limbach *et al.*, 2005; Roduner, 2006; De Temmerman *et al.*, 2012). In some works people define "fractal factors" to study how agglomeration pattern changes with scale in a system (Teixeira, 1988; Brasil *et al.*, 1999; Sorensen and Wang, 1999; Zook *et al.*, 2011). There are other parameters that describe the density of agglomerations such as number density, or mixing related parameters such as intensity of segregation (that describes the deviation of concentration of a part from mean concentration) (Danckwerts, 1952; Ottino and Khakhar, 2000; Kukukova *et al.*, 2009) . Each of these parameters can be useful for a particular problem, but considering the complexity of the topic, they can not completely distinguish and describe different agglomeration patterns and their formation process.

In this work, we adopt and apply network science concepts to analyze agglomeration of particles and provide new insights in the underlying process. The field of network science (Barabási and Albert, 1999; Albert and Barabási, 2002; Newman, 2003; Clauset *et al.*, 2004) has shown its immense ability in

analyzing and understanding problems in a variety of disciplines from physics and biology to social sciences (Pastor-Satorras and Vespignani, 2001; Girvan and Newman, 2002; Rolland *et al.*, 2014).

To analyze our simulation results, we use various techniques from the field of network science. In this field, each element in the system is represented by a node (or vertex), and connections between the elements are considered as links (or edges). In other words, we translate the formed structures/agglomerates in our colloidal suspension to a system of nodes (particles in our system) and links (connection between particles). Using these nodes and links, we can define the "graph" of our structures/agglomerates (see Figure 4.5). Then, having the graph of the structures/agglomerates, we can define the corresponding connection matrix of the graph.

After forming the graph and matrix of the structures (which contain all the information about the connections between particles), we introduce various parameters and concepts from network science which can define our systems. We use these parameters to analyze and compare different stages of agglomeration process in colloidal suspensions.

4.2 Network Science Concepts

In this section we define some network science concepts applied to analyze the simulations.

Structure: When all particles in an agglomeration are in contact with at least one other particle in the same agglomeration (see Figure 4.6 part **a**). In other words, a particle is not considered part of a structure unless it is connected to at least one particle in the same structure.

Degree of a particle: Number of particles in contact with the particle. Average degree of a structure is also defined as the average of the degrees of all particles in a structure (see Figure 4.6).

Shortest path: A path is the sequence of particles such that every consecutive pair of particles in the sequence are connected. The shortest sequence of particles to go from one particle to another defines the shortest path between them.
For example, in Figure 4.6, the shortest path value between **P3** and **P5** is 2,

and the sequence is **P3** to **P4** and **P4** to **P5** (**P3-P4-P5**). It is shown by a black dashed line in Figure 4.6 part **b**. There are other passes to go from **P3** to **P5**, for example **P3-P2-P4-P5** with a value of 3 or **P3-P1-P2-P4-P5** with a value of 4, but they are not the shortest path.

Evolutionary path of average degree: As the agglomeration continues, the average degree of structures changes. We track these changes to define the evolutionary path of the average degree. In this work, we mainly study the evolutionary path of the largest structure (the structure with the highest number of particles) in the system. The evolutionary path can be defined for other quantities (for example the shortest path) as well.

In summary, we start with a colloidal suspension of carbon nanoparticles in which all particles are randomly distributed. Due to attractive interaction forces between particles (for example van der Waals or hydrophobic), particles start to agglomerate. When a number of particles (more than one) agglomerate and come in contact, a structure is formed. At early stages of a simulation many small structures (with small number of particles) are formed. As the simulation continues, agglomeration proceeds and more particles join the small structures, and also small structures agglomerate with each other and form larger ones.

The output of each timestep of our simulation provides a snapshot of the system. We analyze the system, and search for all different structures that are formed (see the definition of a structure above). As the simulation continues and further agglomerations take place, the number of particles in a structure, as well as the number of structures themselves, change. We study the characteristics of the largest structure (the structure with highest number of particles) by calculating relevant network structural parameters, and track the evolution/changes of these parameters as the simulation continues (which defines the "evolutionary path" of that parameter).

For example, the average degree of a structure represents how many particles are on average in contact with each particle in that structure. A higher value for the average degree means that, on average, each particle is in contact with a higher number of particles in that structure. Thus, a higher average degree suggests a more compact (denser) structure. Conversely, a lower average degree suggests a less compact (higher porosity) structure. So, a parameter such as average degree can help to characterize and compare

different structures. More detailed characterization can be achieved by introducing more network science/graph theory parameters.

Since in a structure, all particles are in contact with at least one other particle in the same structure, it is reasonable to define a network system where each particle is a node, and where each two particles in contact with each other define a link. This is a simple translation of an agglomeration (called structure in this work) to a mathematical model. However, as will be explained in following sections, the application of some basic network analysis concepts can yield new insights about agglomeration process.

4.3 Example of Data Analysis

Here, we describe our algorithm for data analysis in more details using simple examples. Generally, at each timestep, we want to determine all the formed structures and all the connections between particles to do further analysis.

The output of our simulations at each timestep contains various information including the position of particles. Using the position, the centre-to-centre distance between each two particles is calculated. If the distance between two particles is larger than the sum of their radii, then those two particles are not in contact.

In terms of network science, each node represents a particle, and if two particles are in contact, we consider a link between corresponding nodes. Then, the "matrix of system" is formed using information of nodes (particles) and links (connection between particles); if two particles are in contact the corresponding *entry* (also called *element*) of the matrix is 1, otherwise it is zero.

As an example, consider five particles in a system with an attractive interaction force between them. At the beginning, particles are separated, and there are no contacts (see Figure 4.1 part **a**). Thus, there is no link between nodes in the corresponding graph of the system (see Figure 4.1 part **b**), and all entries in the system's matrix are zero (see Figure 4.1 part **c**).

As time passes, particles start to agglomerate. Figure 4.2 shows the system at a new state where particles 1 and 2 are in contact. Thus, there is a link between **P1** and **P2** nodes in the graph, and the corresponding matrix entries become 1 (see Figure 4.2 part **c**). The first "structure" in our system is now formed.

The degree of **P1** and **P2** is one, and the average degree of the structure is

also one. The degree of other particles is still zero. One should note that the main diagonal of matrix is always zero because no particle can be in contact with itself.

Figure 4.3 shows another snapshot of the system as agglomeration proceeds. Now, particles 1, 2, and 3 have agglomerated together and formed a structure, and particles 4 and 5 have also agglomerated and formed another structure. If the nodes are labeled properly, one can also see the corresponding "*block*" of each structure in the system's matrix (see Figure 4.3 part **c**). When translating a system of colloidal particles to a graph, nodes can always be labeled in a way that the matrix becomes a "*block diagonal*" where each block corresponds to a structure.
In the larger structure (i.e. the structure with higher number of particles), there are three particles (**P1**, **P2**, and **P3**). The degree of **P1**, **P2**, and **P3** are 2, 1, and 1, respectively. This means an average degree of $\frac{4}{3}$ for this structure.

In Figure 4.4, the larger structure (consisting of **P1**, **P2**, and **P3**) has evolved and "restructured" itself. In the new structure, each of the three particles is in contact with the other two, and thus has a degree of 2. This results in an average degree of 2 for the structure. The higher average degree than Figure 4.3 implies a more compact structure that is formed as a result of restructuring.

Figure 4.5 shows the system when all particles have agglomerated and become part of a same structure. Some details of data analysis for this state of the system are given in Figure 4.6.

When the matrix of the system is formed, it can be used to calculate various parameters of network science. For example, to calculate the degree of each particle, one can consider the corresponding column or row of that particle and add up all the entries; each "1" corresponds to one connection and the sum of all entries gives the total number of connections or the degree of that particle.

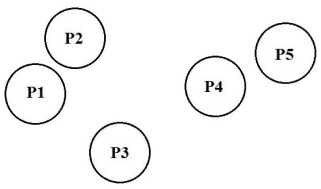

a) System of Particles.

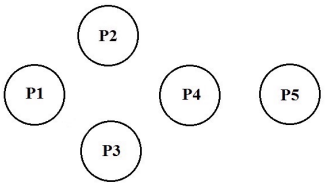

b) Corresponding graph of part a.

	P1	P2	P3	P4	P5
P1	0	0	0	0	0
P2	0	0	0	0	0
P3	0	0	0	0	0
P4	0	0	0	0	0
P5	0	0	0	0	0

c) Corresponding matrix of part b.

Figure 4.1: Example of Data Analysis.

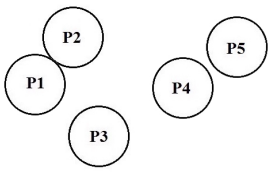

a) System of Particles.

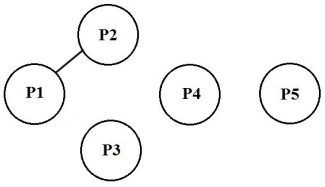

b) Corresponding graph of part a.

	P1	P2	P3	P4	P5
P1	0	1	0	0	0
P2	1	0	0	0	0
P3	0	0	0	0	0
P4	0	0	0	0	0
P5	0	0	0	0	0

c) Corresponding matrix of part b.

Figure 4.2: Example of Data Analysis.

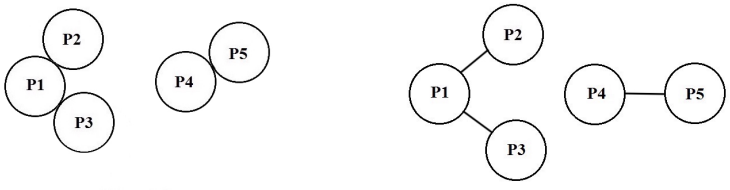

a) System of Particles. b) Corresponding graph of part a.

	P1	P2	P3	P4	P5
P1	0	1	1	0	0
P2	1	0	0	0	0
P3	1	0	0	0	0
P4	0	0	0	0	1
P5	0	0	0	1	0

c) Corresponding matrix of part b.

Figure 4.3: Example of Data Analysis.

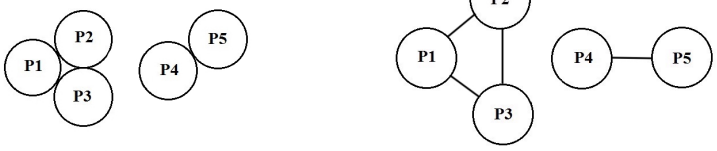

a) System of Particles. b) Corresponding graph of part a.

	P1	P2	P3	P4	P5
P1	0	1	1	0	0
P2	1	0	1	0	0
P3	1	1	0	0	0
P4	0	0	0	0	1
P5	0	0	0	1	0

c) Corresponding matrix of part b.

Figure 4.4: Example of Data Analysis.

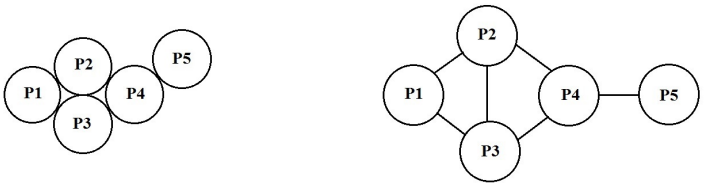

a) Agglomeration of particles.

b) Corresponding graph of part a.

	P1	P2	P3	P4	P5
P1	0	1	1	0	0
P2	1	0	1	1	0
P3	1	1	0	1	0
P4	0	1	1	0	1
P5	0	0	0	1	0

c) Corresponding matrix of part b.

Figure 4.5: Example of Data Analysis.

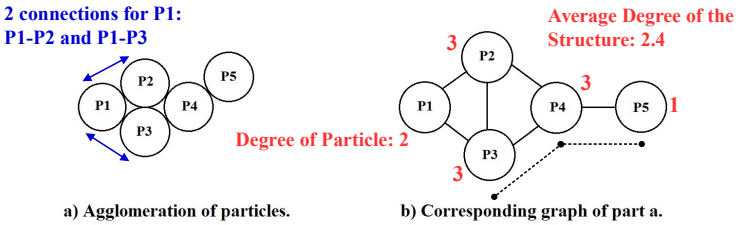

a) Agglomeration of particles.

b) Corresponding graph of part a.

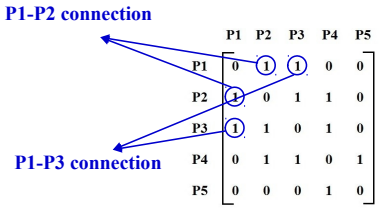

c) Corresponding matrix of part b.

Figure 4.6: Example of Data Analysis.

4.4 Physics Concepts

To understand the results of our simulations, we need to define some physics parameters (such as timescales and lengthscales) in our systems.

For a well distributed (randomly distributed) colloidal suspension, one relevant lengthscale in the system can be defined as the average distance (centre-to-centre) between particles, d_{avg}. This lengthscale is determined by the particle number concentration in the system.

We further define a timescale for this system as the time for agglomeration of two particles with a separation of d_{avg}. We call this timescale the agglomeration timescale (t_{agg}). Beside the system characteristic such as the average separation between particles d_{avg}, the agglomeration timescale also depends on the interaction force between two particles both in terms of the magnitude of the force and the shape of the force function.

Another concept to be defined is the "*spatial effectiveness of the force*". For two particles at a particular separation, a force is more effective than the other when the agglomeration time of particles, interacting via that force, is smaller. In general, in a colloidal suspension, a force with higher magnitude for a longer range can be more effective. However, the situation is usually more complex for real physical forces because of different shapes of the force functions. A force can have higher magnitude but be shorter range (drop quickly), or vise versa. Thus, a force may be more effective than another for a particular range of separations between particles, while less effective for larger or smaller separations. In other words, in addition to the shape and magnitude of the force, some other "system characteristics" such as the separation between particles are also required to characterize the effectiveness of the force. Altogether, the spatial effectiveness of a force is a concept that allows the comparison of two or more forces for a particular state of the system.

We also need to introduce another timescale that we call it as "*restructuring timescale*", t_{restr}. A "*structure*" is formed when all particles in an agglomeration are in contact with at least one other particle in the same agglomeration. After a structure is formed, the position of particles in the structure can still change with respect to each other. In other words, restructuring can happen. Restructuring is a function of different parameters such as the force between particles, the current positioning of particles, and the shape of the particles etc. Given enough time, a structure will reach a point that no restructuring can happen anymore without an external stimu-

lus. The restructuring timescale is a representation of the time required to restructure.

To explain different agglomeration patterns, one should consider the agglomeration and restructuring timescales, as well as the available time for agglomeration and restructuring. These timescales and available times can help analyze the agglomeration patterns in a system.

4.5 Effect of Force on Particle Agglomeration

We consider different forces in our simulations. These forces are based on the typical physical forces (such as van der Waals, hydrophobic, electrostatic, etc.) that two carbon nanoparticles in a colloidal suspension similar to catalyst layer ink may be subjected to. Different parameters have to be defined for each force, and we consider some typical values for these parameters. Our goal is not to define the exact force between two carbon nanoparticles, but to capture the main features (order of magnitude and shape of force function) of the forces.

In this work, only carbon nanoparticles are explicitly considered in the simulations (i.e. we do not consider other components in the suspension such as polymer molecules). Since this, to the author's best knowledge, is the first implementation of network science analysis to study particle agglomeration in this field, we needed to start with simple systems (i.e. only carbon particles in the system) to be able to understand and interpret our analysis results. Resolving the polymer phase in our simulations (which also requires modeling polymer structure in the system) is beyond the scope of this work. However, future works can add more complexity to the system and expand our understanding based on what we find in this work.

In this chapter, simulations of agglomeration of carbon nanoparticles are analyzed for systems driven by two main interaction forces, van der Waals and hydrophobic, which are dominant attractive forces between carbon nanoparticles in a colloidal suspension similar to catalyst layer ink (see section 3.4 for details).

Although not presented here, an order of magnitude analysis on other forces has for example indicated that even if polymers were considered, a force such as depletion would be much smaller than van der Waals or hydrophobic in systems of interest.

Also, we have ran simulations of nanoparticles agglomeration where dif-

ferent ratio of particles were assumed to be charged on the surface (with similar order of magnitude of electrostatic interaction if they were covered by polymer in CL ink). In other words, beside the attractive interaction force between all particles, a repulsive electrostatic force was also defined between some of the particles. We have found indications that some of the charged particles were present inside the agglomerations. Although it was simplistic and the polymer was not resolved (so other related forces such as polymer related steric repulsive force were ignored), this could be a hint in support of some of the new findings of penetration of polymer into carbon agglomerations in catalyst layer inks (Kusano *et al.*, 2015). However, a more comprehensive study with more details is required for this topic which can be the subject of a future work.

The main goal of this project is to improve fundamental understanding of the agglomeration process. In a colloidal suspension, particles will agglomerate because of the presence of attractive forces between particles. Different materials will have different interaction forces, both in terms of magnitude and the shape of the force function. How will this change the agglomeration pattern?

There are a number of other questions related to the role of interaction potentials. First of all, many works define the interaction between their particles using potential models such as Lennard-Jones, a model which works well at the atomic level, and has consequently been used to define the interaction for larger colloidal particles. As will be discussed in the following sections, the exact profile of the force does play an important role in the final patterns of agglomeration. Thus, for precise studies on agglomeration, one should consider the realistic physical forces for that particular system, rather than a commonly used potential model which may not represent the real characteristic of the system.

Furthermore, when a factor (such as force magnitude or the shape of force function) does change the agglomeration pattern, studying how these changes happen can help to achieve a more fundamental understanding of agglomeration process itself.

Before proceeding to the next sections, we pose a question. Consider a colloidal system of carbon nanoparticles similar to catalyst layer ink. The particles radius is 20 nm, and the attractive force between them is the van der Waals. Due to the attractive force in this system, randomly distributed particles will agglomerate and form some structures. Now, consider the same system, with the same parameters, except for a stronger force magnitude.

How would the agglomeration pattern evolve in this new system? In other words, does the stronger force magnitude result in agglomerations that are more compact or less compact? One may expect the stronger force and attraction between particles would result in more compact structures. Counter intuitively, as discussed in the following sections, this is not necessarily the case.

4.5.1 Force Magnitude

To check the effect of the force magnitude, we introduce a factor x_f which changes (strengthens or weakens) the force in our simulations by its corresponding value. In general, for systems with high friction where particle's energy can be taken out easily (for example a colloidal suspension similar to the CL ink), strengthening the force up to some values can result in faster agglomeration of particles. One should note that in a colloidal suspension similar to CL ink, the system is in the Stoke regime (i.e. Reynolds number $\ll 1$), so the above mentioned assumption is relevant. (In other words, the viscosity or friction force is so high that the particle's velocity/kinetic energy can be dissipated quickly. Otherwise, when the friction is not dominant, the related settlement timescales are usually higher for systems with stronger forces. That is because stronger forces result in higher kinetic energies that should be taken out of the system through a dissipation mechanism before reaching a new equilibrium state, and when the friction is not significant compared to the driving force, the dissipation time is longer.)

Also, when the interaction force between particles is attractive, restructuring process usually makes the structure denser, eventually. In other words, restructuring results in an increase in the average degree of the structure. For a given structure (with no further agglomeration), strengthening the force can increase the average degree of the structure to even higher values when enough time for complete restructuring is given.

However, during the agglomeration process (when the number of particles in a structure changes), increasing the force magnitude changes the evolutionary path (going from initial small structures to final large structures) of average degree differently.

In a colloidal suspension with attractive interaction force, the number of particles in a structure increases with time as agglomeration continues. In general, adding one particle to a structure (which will be added to outer layers of a structure where particles with lower degrees are) can reduce the average

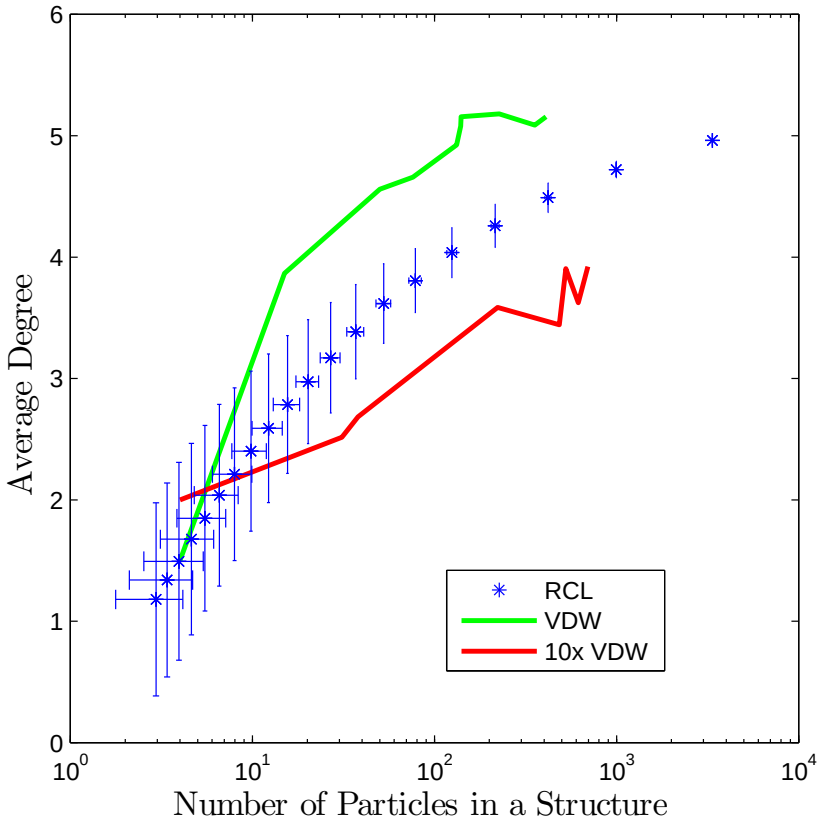

Figure 4.7: Agglomeration of spherical carbon nanoparticles under different force magnitudes. Green (top) and red (bottom) lines show the evolutionary path of average degree under van der Waals and 10 times van der Waals interaction potential, respectively. The evolutionary path is for the largest structure in the system. The volume concentration of particles in both simulations is around 0.035. The blue data corresponds to a reconstructed catalyst layer of a fuel cell.

degree of a large structure. In the mean time, restructuring helps to increase the average degree. The competition between these different timescales can change the evolutionary path of the average degree of an agglomeration from a small (low particle number) to large (high particle number) structures.

Figure 4.7 shows the results of two simulations of agglomeration of spherical carbon nanoparticles (of 20 nm radius). In one simulation, the interaction between particles is the van der Waals force, and in the other the interaction is 10 times the van der Waals force. By increasing the magnitude of a force, in our case (i.e. van der Waals force and identical spherical particles), the restructuring timescale changes (decreases) less than agglomeration timescale. This results in the formation of structures that grow in number of particles, but did not have enough time to completely restructure. This causes the lower average degree values for the evolutionary path of structures. On the other hand, when the magnitude of a force is reduced, the structure has more time to restructure before new particles are added. So, larger structures are formed from smaller structures that have higher average degrees. Thus, the evolutionary path of the average degree will tend toward higher values.

For longer range forces, more/faster restructuring happens. The more/faster restructuring results in increasing the average degree, so the above mentioned effect (change of the evolutionary path of average degree toward lower values when the force magnitude is increased) is reduced for these forces. In other words, the more/faster restructuring (that increase the average degree) can compensate the effect of higher rate of adding particles (that reduces the average degree) for these cases.

Thus, one should note that although for an isolated structure, increasing the force magnitude can result in a higher average degree as restructuring is completed, the agglomeration process under a stronger force is different. Increasing the force does not necessarily increase the average degree of the final structure. When a structure is formed and evolved as a result of agglomeration, we can end up with a final structure that has a lower average degree (even after giving enough time for restructuring). This is because the whole structure has been formed as a less compact structure while stable enough against restructuring. This is more possible for forces with shorter range (quick drop/fast decay). In these cases, a particle mainly feels the particles around it (the first layers around the particle), and other particles in the structure that are further away (but still a part of the structure) do not have a significant effect on restructuring/repositioning of the particle. Thus, when a stable structure (with a local minimum in potential, and not

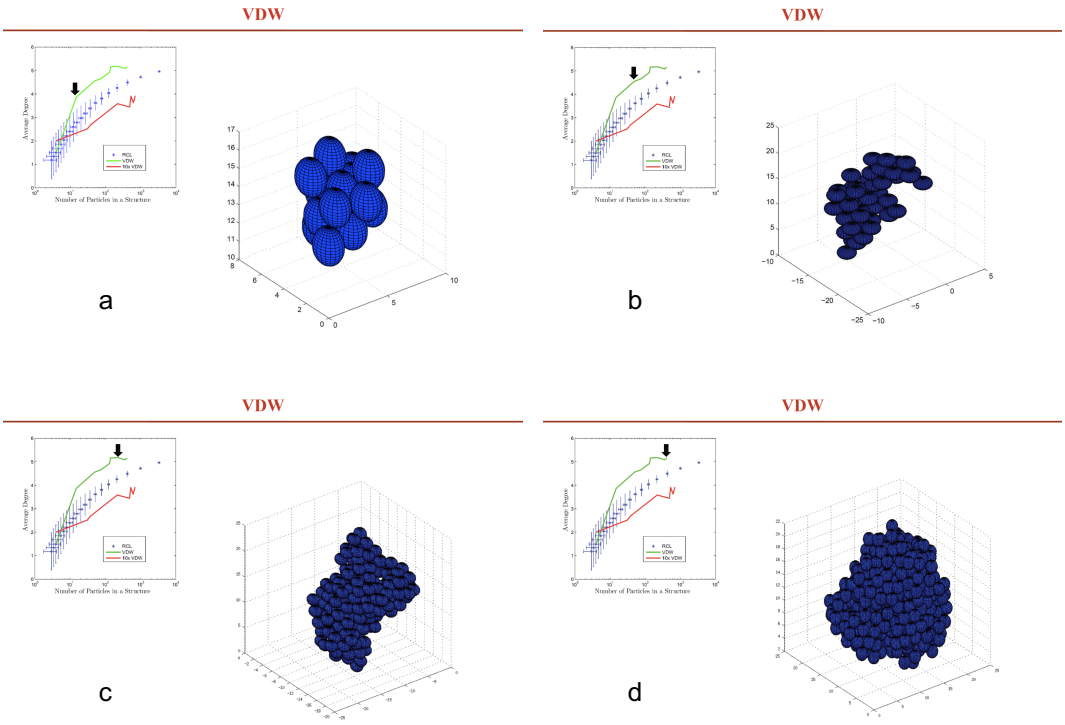

Figure 4.8: Examples of the largest structures formed during a simulation at different timesteps. The interaction force between particles is van der Waals. The plot of the evolutionary path of average degree is also shown for each structure. The corresponding location on the evolutionary path of average degree is shown by an arrow for each structure. As simulation continues (from a to d), the number of particles in the largest structure increases and the average degree of the structure evolves.

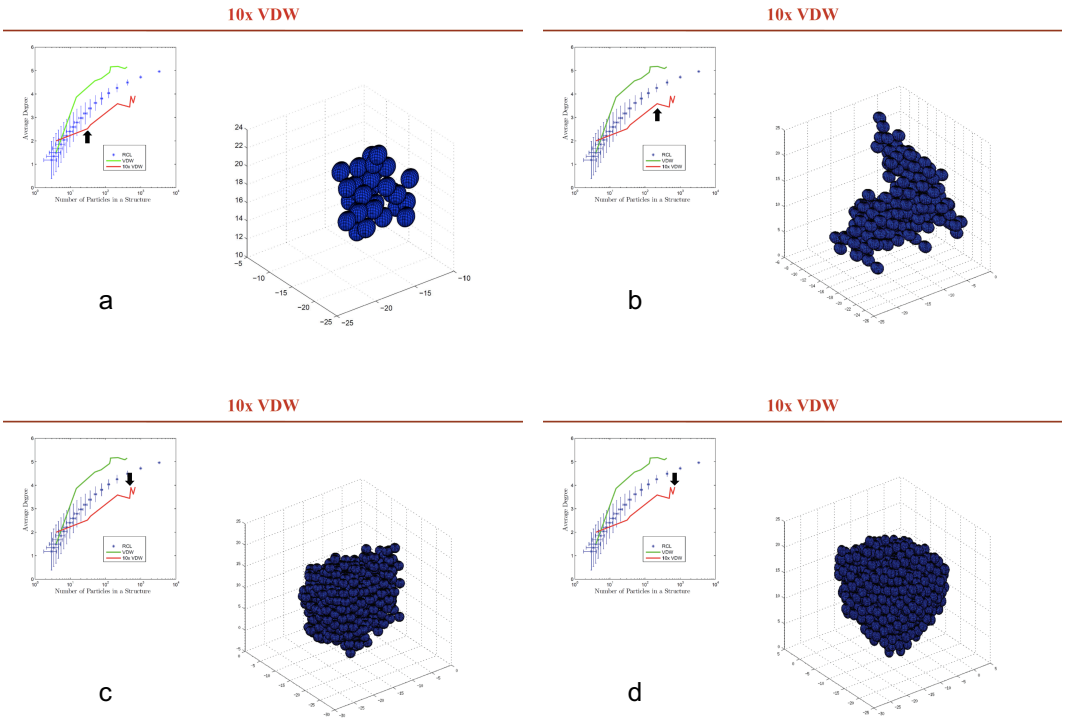

Figure 4.9: Examples of the largest structures formed during a simulation at different timesteps. The interaction force between particles is 10 times van der Waals. The plot of the evolutionary path of average degree is also shown for each structure. The corresponding location on the evolutionary path of average degree is shown by an arrow for each structure. As simulation continues (from a to d), the number of particles in the largest structure increases and the average degree of the structure evolves.

necessarily "the minimum" of potential for the system) is formed, it can keep its structure against restructuring, and the outcome is a structure with lower average degree. So, a structure with higher porosity can be formed as a result of agglomeration under a stronger force with short range. This type of force acts more like a "glue" between two particles and does not have a significant effect on particles further away.

Before proceeding to the next section, it is useful to illustrate the structures that form in our simulations. Figure 4.8 shows examples of the largest structures that are formed during a simulation at different timesteps. The interaction force between particles is van der Waals. The plot of the evolutionary path of average degree is also shown for each structure. The corresponding location on the evolutionary path of average degree is shown by an arrow for each structure. As the simulation proceeds (from a to d), the number of particles in the largest structure increases and the average degree of the structure evolves. Figure 4.9 is similar to Figure 4.8 but for the case of 10 times van der Waals as the interaction force.

4.5.2 Shape of the Force Function

To understand the agglomeration of particles, different timescales should be studied. The ratio between these timescales can define the agglomeration pattern. The shape of the force plays a key role in defining these timescales.

A force with a longer range can reduce t_{agg}. This means new particles can be added to a structure at higher rates. This can reduce the average degree of the structure. A longer range force also helps the restructuring, which can increase the average degree of the structure. Thus, the overall effect of the force shape should be studied along with other parameters of the system that can change at least one of these timescales (such as concentration, or shape of the particles).

As an example, we consider typical profiles of van der Waals and hydrophobic forces (see Figure 4.10). For the stability of our simulations, we cut the potentials at $r = 1.01$. This makes their magnitude comparable at $r = 1.01$. The choice of other parameters (still within the meaningful physical range) makes the hydrophobic force more effective for smaller (less than a particle radius) separations. One should note that for larger separation (for example in a dilute system), van der Waals force can be more effective than hydrophobic. In the range of concentrations that we are interested in, the results of our simulations suggest that using hydrophobic

force can change the evolutionary path of average degree of structures to lower values at early stages of agglomeration (see Figure 4.11). This means the ratio of *(agglomeration timescale)/(restructuring timescale)* is smaller for the case of hydrophobic force at early stages of agglomeration. However, as

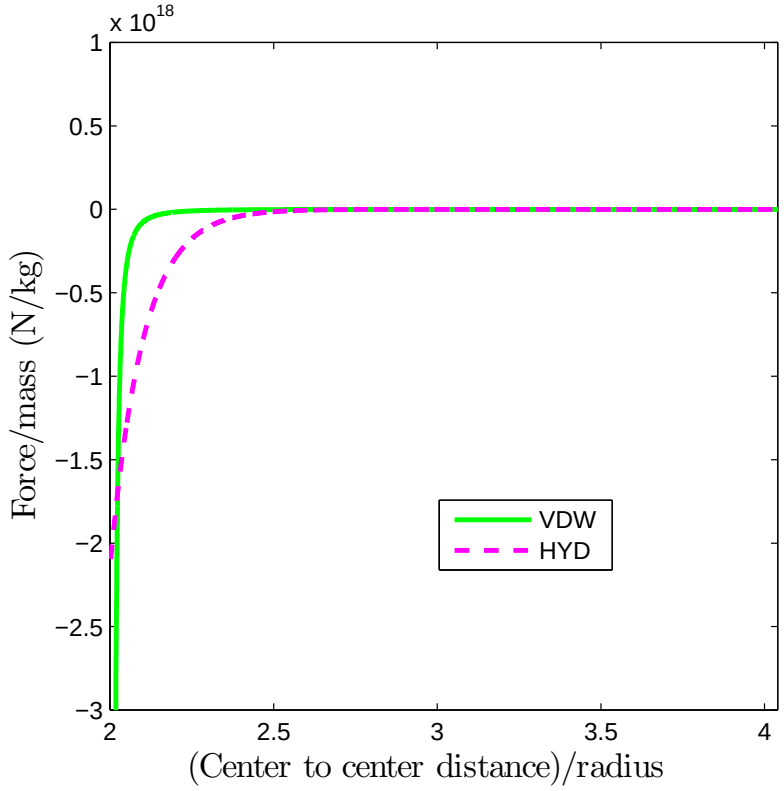

Figure 4.10: Shape of the force function. The green solid and the magenta dashed lines correspond to the van der Waals and hydrophobic forces, respectively. Forces were calculated between two spherical carbon particles with radius of 20 nm.

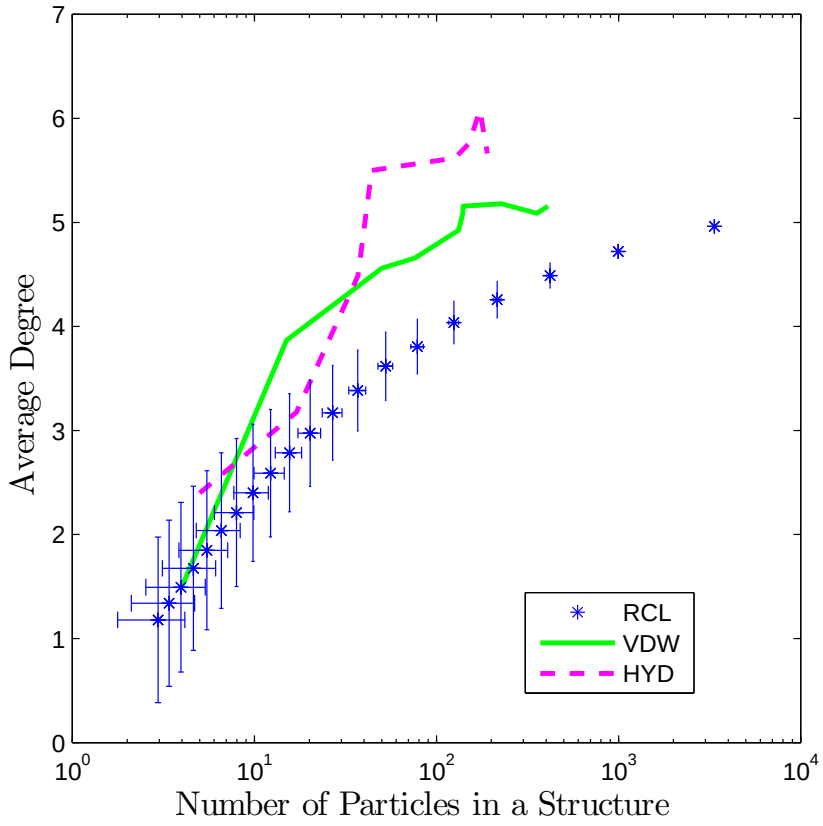

Figure 4.11: Agglomeration of spherical carbon nanoparticles under different shapes of the force function. Green solid and magenta dashed lines show the evolutionary path of average degree under van der Waals and hydrophobic forces, respectively. The evolutionary path is for the largest structure in the system. The volume concentration of particles in both simulations is around 0.035. The blue data corresponds to a reconstructed catalyst layer of a fuel cell.

the agglomeration continues, restructuring happens more effectively and the evolutionary path of the average degree increases to higher values for the case of hydrophobic force.

If the force is a very long range force, the restructuring can overcome the higher rate of adding particles even at early stages of agglomeration, and its evolutionary path for average degree tends to higher values (rather than lower values in the case of Figure 4.11) shortly after agglomeration started.

Once again, it is a competition between restructuring and the rate of adding particles. A force with a longer range accelerates restructuring and at the same time increases the rate of adding particles. If adding particles wins, the evolutionary path of average degree will tend toward lower values, while if restructuring wins, the evolutionary path of average degree will tend toward higher values.

This study also shows the importance of considering the "real" interaction force on agglomeration patterns. Thus, using a general potential model (such as Lennard-Jones model) as the interaction between particles is not adequate when studying the agglomeration process in colloidal systems.

4.6 Effect of Concentration on Particle Agglomeration

Concentration is one of the most important properties of the system to define the evolutionary path of structures. Concentration defines the average distance between particles, d_{avg}, directly. So, the agglomeration timescale depends strictly on the concentration.

Moreover, in a colloidal suspension of specific material and solution, the force between particles is mainly defined. However, one can change the evolutionary path of structures by controlling the concentration for the same system of materials. This underscores the importance of concentration in the agglomeration of particles.

In general, higher concentrations results in smaller t_{agg}. This means a higher rate of adding new particles to the structure (which reduces the average degree), and the structure has less time for restructuring. Thus, the evolutionary path of the average degree tends to lower values (see green solid and red dashed lines in Figure 4.12). This can result in formation of structures with higher porosity (less compact).

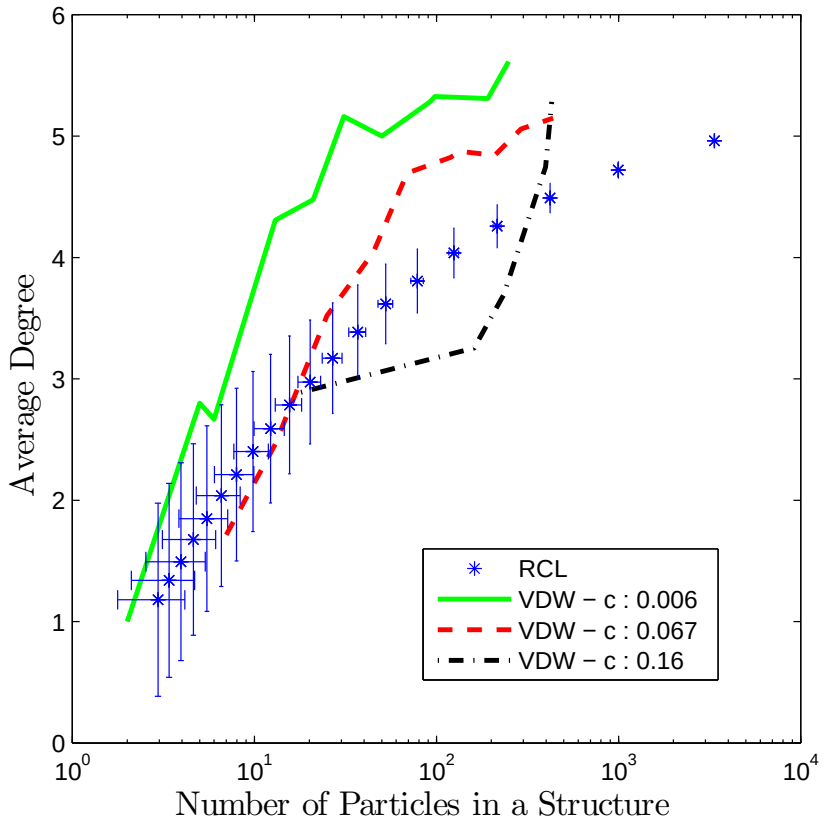

Figure 4.12: Agglomeration of spherical carbon nanoparticles under different concentration. The force is van der Waals for all cases. The parameter c is the volumetric concentration of particles. Green solid, red dashed, and black dotted-dashed lines represent the evolutionary path of average degree for different concentrations. For comparison, the case of the green solid line has similar concentration to some conventional catalyst layer ink formulas in the literature. The blue data corresponds to a reconstructed catalyst layer of a fuel cell.

One should note that the basis of this analysis is for a system that starts as a randomly distributed colloidal suspension. Thus, our results suggest that to make a structure with higher porosity (less compact), one should increase the concentration while keeping particles apart (prevent particles from agglomeration) using different techniques such as sonication or ball mill grinding.
A practical use of this result can be in fuel cell technology. To form an uniformly distributed catalyst layer ink, particles are separated by sonication. When the sonication ends, particles start to agglomerate. To achieve a structure with higher porosity, the agglomeration process should start when the concentration of carbon particles is high enough. One can either start with lower amount of solution, or evaporate the solution while sonicating (or while any other grinding/mixing technique is running). The goal is that agglomeration begins when concentration has increased.

One should also note that there can be a breaking point for the above trend. For very high concentrations, while the evolutionary path of average degree tend to lower values at early stages of agglomeration, a rapid increase in average degree can happen as a result of agglomeration. This can increase the average degree to even higher values than one would expect for the same system with lower concentrations (see black dotted-dashed line in Figure 4.12). This happens because at very high concentrations, the agglomeration timescale is very short which results in a very short time for restructuring. A too short restructuring time results in the formation of "fragile" structures with low average degrees (less compact) that can collapse to much denser (more compact) structures as they agglomerate with each other.
In other words, for low or moderate concentrations, structures have more time for restructuring. Thus, they form more stable structures that have less tendency to restructure after agglomerating with other structures. When, the concentration is very high and structures do not have enough time to restructure, a collapse in structures after agglomeration can be expected which can result in a sudden increase in the average degree.

4.7 Effect of Drag on Particle Agglomeration

When a particle is moving in a fluid medium, it feels a resistant force in the opposite direction of its relative velocity to the surrounding medium. This force is called the *drag force*, and it depends on the properties of the fluid,

shape and size of the particle, and the relative velocity.

The functional dependence of the drag force on velocity changes as the magnitude of velocity varies. At very high velocities (high Reynolds numbers), the drag force is proportional to the square of the relative velocity, while at low velocities (low Reynolds number) it is proportional to the velocity (it is also called *linear drag*). Thus, at low velocities the drag force can be approximated as follows:

$$F_{Drag} = -\beta V \tag{4.1}$$

where F_{Drag} is the corresponding force, V is the velocity, and β is a coefficient that depends on the properties of the fluid and the dimensions of the object.

For the case of spherical particles moving with low velocities in a fluid medium, the drag force is given by **Stokes' Drag** formula:

$$F_{Drag} = -6\pi\eta r V \tag{4.2}$$

where η is the dynamic viscosity, and r is the radius of particle. One should note that the above relation is based on the assumption that particles do not interfere with each other (in other words, it is more appropriate for a single particle or very dilute systems). For a detailed study of a system of particles in a fluid medium, a complete solution to **Navier-Stokes** equations is required. One way to do this is to use CFD (Computational Fluid Dynamic) simulations. However, since we are using an N-body code in this work and we cannot resolve the fluid medium, a linear approximation for the drag force is considered.

Thus, we define a velocity dependent drag force in our simulations to partially capture the hydrodynamic effects of the solvent medium. The drag force acceleration is defined as:

$$a_{drag} = -f_d(V_i/dt) \tag{4.3}$$

where V_i is the initial velocity at the beginning of the timestep, dt is the timestep, and f_d is a coefficient that we call it the "drag coefficient". The drag force is defined in a way that at each timestep, a fraction (between 0 to 1 that is determined by f_d) of the initial velocity of the particle will be taken out during the timestep.

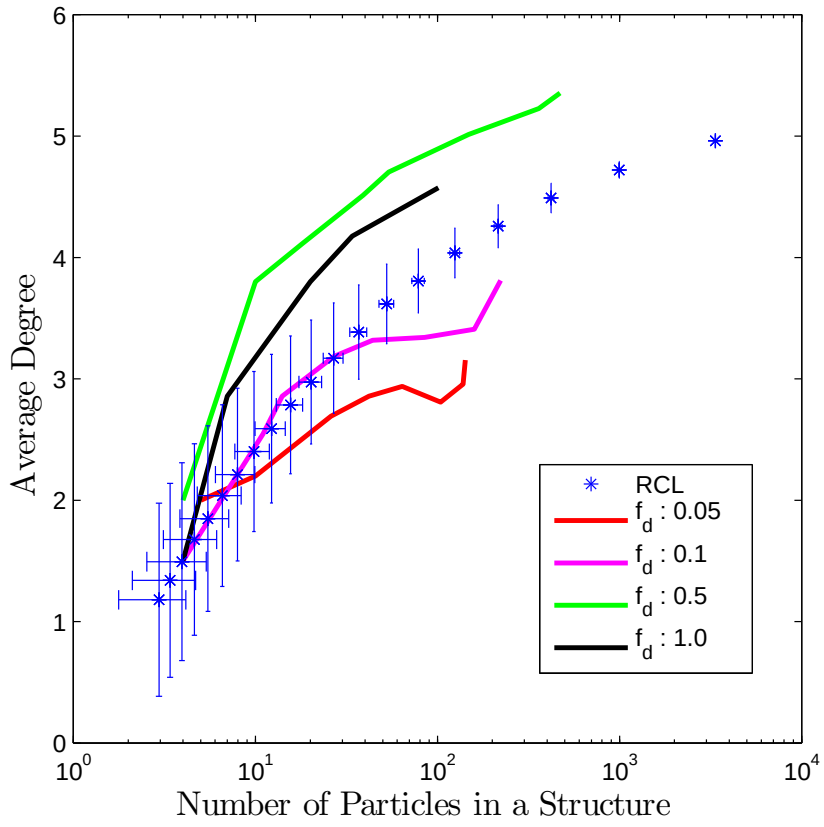

Figure 4.13: Agglomeration of spherical carbon nanoparticles under different drag coefficients. The force is van der Waals for all cases. The parameter f_d is the drag coefficient. Red (bottom), magenta (second from bottom), green (top) and black (second from top) lines correspond to the average degree evolutionary path of cases with f_d of 0.05, 0.1, 0.5 and 1.0, respectively. The blue data corresponds to a reconstructed catalyst layer of a fuel cell. The timestep was $dt = 5 \times 10^{-11}$, and the volumetric concentration of particles was $c = 0.035$ for all cases.

When there is no drag/friction in our simulation, there is no other way for particles to lose energy, thus no agglomeration happens. One should note that for $f_d = 0$, the agglomeration time is infinity. As we increase the drag coefficient from zero, the agglomeration starts to happen.

For low drag values, it takes a very long time for particles to lose energy. Particles move around each other, collide with each other and bounce back many times before they lose enough energy to be able to agglomerate. Thus, before agglomeration, particles become closer to each other while losing energy, and form regions that have locally higher concentration of particles. So, the effect of very low drag force is similar to starting the agglomeration from a higher concentration which results in structures with lower average degrees. Indeed, agglomeration does not start significantly until enough time passes and particles lose their energies. So, for lower drag coefficients, structures are formed later, and there will be less time for restructuring. As drag coefficient increases from lower values, agglomerations are formed earlier, and there will be more time for restructuring. This results in structures with higher average degrees (see corresponding lines for f_d of 0.05 and 0.1 in Figure 4.13).

On the other hand, there is an optimal value for the drag coefficient that minimizes the agglomeration timescale. After some value, increasing the drag coefficient increases the agglomeration timescale. That is because the average velocity of particles is reduced, and it now takes longer for particles to get together. Thus, structures are formed later, and there will be less time for restructuring. This can result in structures with lower average degrees (see corresponding lines for f_d of 0.5 and 1 in Figure 4.13).

One should also note that in a colloidal suspension similar to CL ink, the system is in the Stoke regime (i.e. Reynolds number $\ll 1$). Thus, it is more relevant to assume very high drag forces for these systems. Also, as noted before, the hydrodynamic interaction is a long range phenomenon, and the presence and movement of a particle can affect the movement of other particles. While we tried to partially capture the hydrodynamic effects of the solvent medium by introducing a drag force, the complete effect of the fluid medium remains to be studied with a simulation method that fully resolves and couples the hydrodynamics and interparticles dynamics.

4.8 Discussion on Understanding about Agglomeration Process

To be able to explain the results of our simulations, network science analysis helped us to develop a new understanding about agglomeration process. In this new insight, we consider the full structure formation process as two steps: first, separated particles get together and form a structure, with a corresponding timescale that we call the "agglomeration timescale", t_{agg}. Second, the formed structures can restructure due to interaction between particles and evolve to a new structure if enough time is given. We call the corresponding timescale for this step the "restructuring timescale", t_{rest}. The full structure formation process depends on these two timescales, and corresponding available times for each step. So, for now, there are four different parameters related to time (t_{agg}, available time for agglomeration, t_{rest}, and available time for restructuring) that can help us to understand the agglomeration process.

Moreover, each step has its own specifications. First of all, the agglomeration step (first step) should happen first. Without any formed agglomeration, there can not be any restructuring. This also means that if agglomeration is happening, the available time for agglomeration should already have been larger than agglomeration timescale (otherwise, there would not be any agglomeration in the first place). So, comparison between the agglomeration timescale and the available time for agglomeration is mainly to check whether the process happens/starts or not.

On the other hand, when a structure is formed, it has some time to restructure, before further agglomeration happens. This means the available time for restructuring is indeed defined by agglomeration timescale, t_{agg}. Thus, the whole picture can be explained with the two timescales, t_{agg} and t_{rest}. However, when comparing different cases, the idea of available time for restructuring (which is defined by t_{agg}) can help for better intuition.

One should also note that the agglomeration process is a continuous and dynamic phenomenon. For example, the corresponding timescales change as the system evolves and more agglomerations happen. Moreover, agglomerations of larger structures together introduce new patterns that require more detailed analysis (see following sections). So, for a more precise picture, a range of agglomeration and restructuring timescales for various structures at each moment should be defined. Despite this fact, we have shown that even

considering average timescales can still help to explain the general behavior of the system.

There are also different parameters that affect t_{agg} and t_{rest}. For example, the restructuring timescale for a given structure is mainly defined by the interaction force between particles. Thus, system characteristics (such as concentration) do not play a significant role. However, for agglomeration timescale, the interaction force is important as well as system characteristics. Thus, changing some parameters can change both timescales, while some other parameters only change one of them effectively.

Another note is that in the process of restructuring, a local minimum in potential is reached which is not necessary the absolute minimum of potential. In the dynamic process of agglomeration, there are many configurations which can be stable (a local minimum in potential), and agglomeration process can go in any of these evolutionary paths. The final path can be determined by tuning the rate of adding particles (t_{agg}) based on restructuring timescale (t_{rest}) in the system. The idea of the structure formation related to a local minimum in potential is similar to "kinetic trapping" in self-assembly processes (Hua *et al.*, 1995; Hagan *et al.*, 2011; Shin *et al.*, 2012; Yan *et al.*, 2016). Self-assembled systems can experience various pathways of structure formation due to kinetic trapping. This can lead to the formation of new types of structures, as well as new functions of the system. The formation of blood clot from blood platelets when a tissue is cut is a good biological example of how kinetic trapping can introduce a new functionality of a system. (Born, 1962; Yan *et al.*, 2016). Thus, rather than only structures that are in the "thermodynamic equilibrium state" (or the absolute minimum of potential of the system), a variety of patterns and structures can be formed by various pathways enabled by kinetic trapping (or local minimums of potential). By controlling system's conditions, one can influence the pathway of system's evolution to reach a desired state (Hagan *et al.*, 2011).

Overall, adding a new particle to a structure reduces the average degree because the particle is usually added to outer layers of a structure where particles with lower degrees are. On the other hand, restructuring in systems with attractive force increases the average degree. Thus, any change in the system that increases the rate of adding particles without reducing restructuring timescale correspondingly, results in less time for restructuring and makes structures less compact.

4.9 Further Network Analysis: Shortest Path

The shortest path is another useful parameter to study the agglomeration of particles. If we divide a large structure to subdomains (or blocks), the shortest path depends on both the "local" positioning of particles, and connections of these subdomains or blocks with respect to each other.

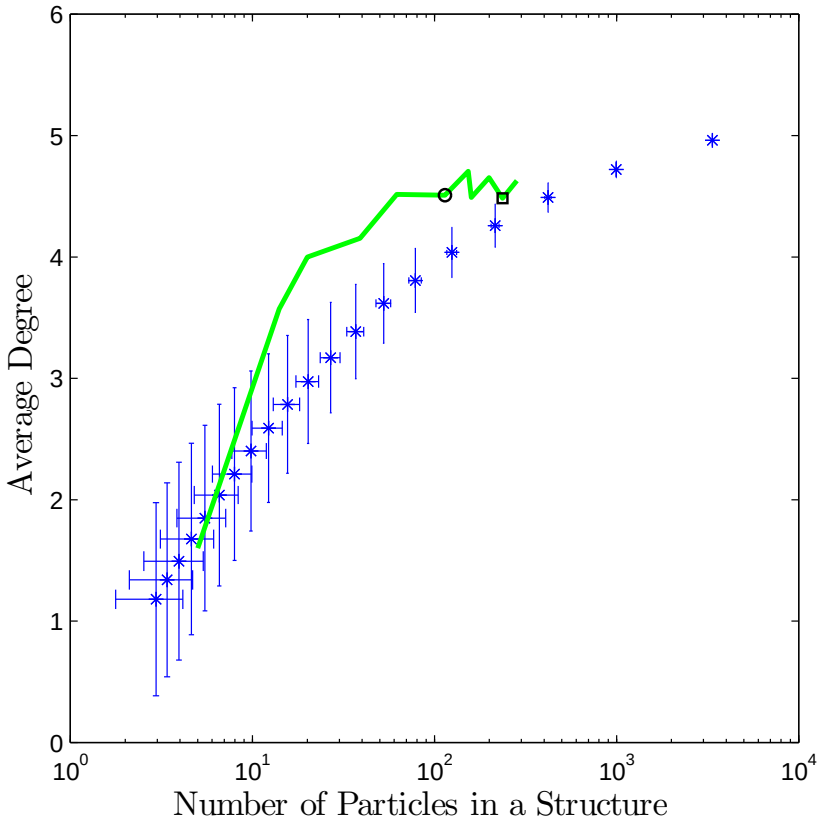

Figure 4.14: Evolutionary path of the average degree for a simulation of particle agglomeration under van der Waals force.

Generally, for the systems considered (i.e. agglomeration of particles in a colloidal suspension), and for small structures (or subdomains) with similar number of particles, average degree and shortest path have inverse correlation. This means, in general, as the average degree increases (so there are more connections between particles), the shortest path decreases and vice versa. However, for larger structures, the connection between subdomains (or blocks) becomes important too. Consider two same structures. The average degree and average shortest path are the same for the two structures. Now, if these two structures are connected through only one particle from each structure, the average degree of the new larger structure is about the same as the average degree of each substructure (subdomain, or block). However, the average shortest path for the new larger structure increases significantly. As more particles from two subdomains get connected, the average shortest path starts to decrease.

Thus, when studying the average shortest path for a structure, both local positioning of particles, and also the connection between subdomains (or blocks) become important. While the local positioning of particles can be analyzed by average degree, studying the average shortest path can give us some "non-local" structural information which can not be obtained only by the average degree. In other words, the average shortest path can be considered as a "global" ("non-local") structural parameter, while the average degree is mainly a local structural parameter.

As an example, consider Figures 4.14 and 4.15. These figures show the evolutionary path of the average degree and average shortest path for a simulation of particle agglomeration under van der Waals force. Two points are marked in each figure with circle and square markers. The circles refer to the same instant in our simulation, similarly for the two squares. The average degree of structures does not change significantly from circle to square marker. However, the average shortest path of structures changes dramatically as can be seen in Figure 4.15.

Considering both figures together, one can infer that from circle to square marker, an elongated structure is formed from agglomeration of structures with similar average degrees. That is why the number of particle in the structure increases while the average degree does not change significantly and the shortest path increases dramatically.

Figure 4.16 shows the corresponding structures of circle and square markers. Again, one can see that the average shortest path increases dramatically as structures agglomerate and form an elongated structure. As time passes,

the elongated structure can restructure to a more compact structure with an smaller average shortest path.

Similarly to Figures 4.14 and 4.15, in many of our simulations the evolutionary path of the average degree is higher than those of RCL (reconstructed catalyst layer) data while the average shortest path is also higher or comparable to those of RCL (or, the average degree of the simulation is comparable

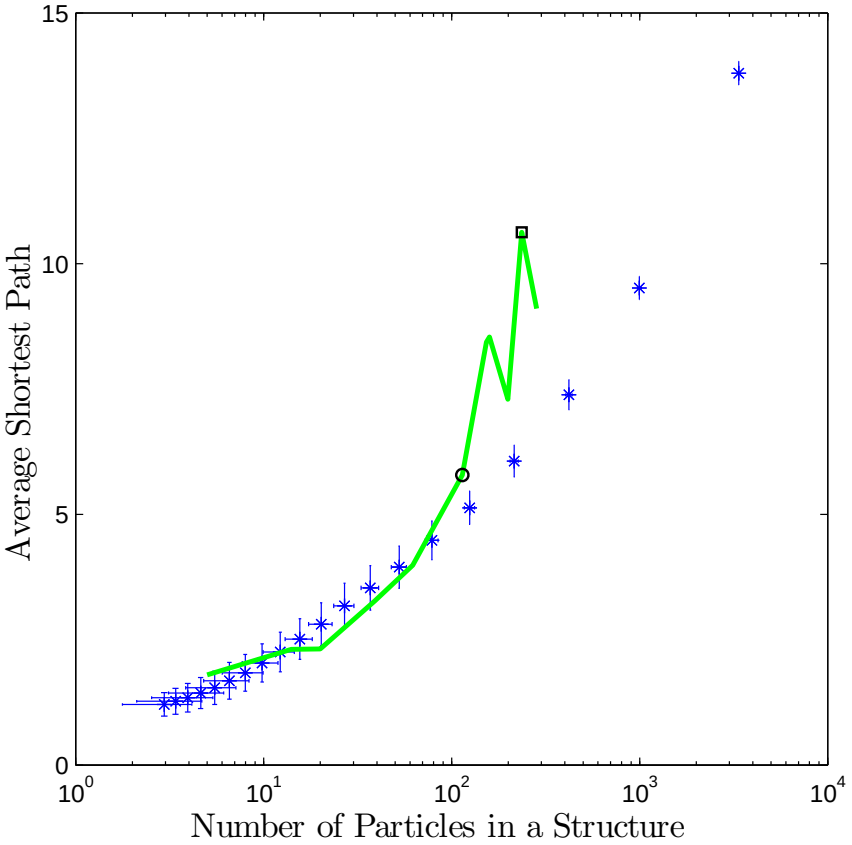

Figure 4.15: Evolutionary path of the shortest path for a simulation of particle agglomeration under van der Waals force.

to RCL data, while the shortest path is higher than RCL data).

One explanation is that in the simulation results, different subdomains (or blocks) are connected through a "bottleneck" type of connection. Thus, although subdomains (or blocks) have higher average degrees than the RCL (which could result in lower values of average shortest path), the bottleneck type of connection between subdomains increases the average shortest path (and makes it comparable to or higher than RCL results).
In other words, one can say that the RCL is formed from blocks with lower average degree than some simulation results (which can result in higher short-

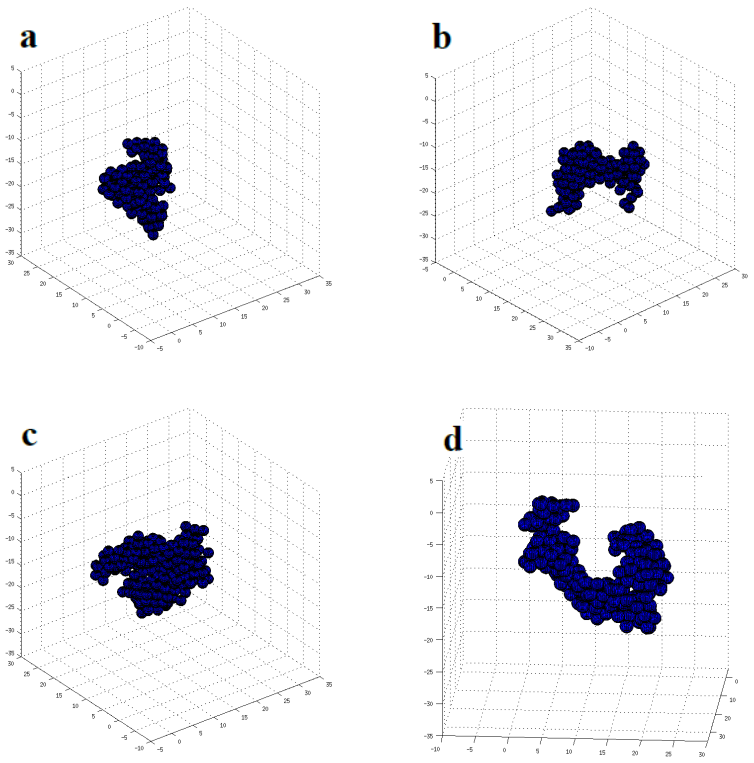

Figure 4.16: Corresponding structures of circle and square markers in Figures 4.14 and 4.15. Part **a** and **b** show the structure related to the circle marker from two different angles. Part **c** and **d** show the structure related to the square marker from two different angles.

est path), while these blocks are connected through more particles (than the simulation results) which reduces shortest path, and overall, the shortest path for the RCL and simulation results become comparable. The connectivity of blocks in RCL with high number of particles in contact, can be a result of the drying process of CL.

The above mentioned effect (higher average degree with comparable average shortest path) depends on the concentration, and it vanishes as the concentration decreases. For dilute systems, the structures can have higher average degree, and also lower average shortest path. This can be explained as the longer time that the structure has for restructuring which changes the connection between substructures to a wider (with more particles in contact) connection.

A physical quantity that can be described by combining shortest path value with other parameters is the conductivity. In structures such as catalyst layer of fuel cells formed from carbon nanoparticles, the electron conductivity is an important quantity in defining the device performance.

4.10 Network Analysis of Reconstructed Catalyst Layer: Degree Distribution

From previous works in our group (Lange *et al.*, 2012; Singh *et al.*, 2014), we have a reconstructed catalyst layer (RCL) based on experimental characterization of a real catalyst layer. A focused ion beam (FIB) and a scanning electron microscope (SEM) were used to acquire a series of high resolution images of catalyst layer. FIB was used to slice the CL material while SEM was used to obtain images of the surface of the material. With the help of two different correlation functions of physical properties, data from FIB/SEM was optimized to numerically reconstruct a multiphase catalyst layer domain. We have studied this RCL using network analysis.

The blue data shown by asterisk marker in Figures 4.17 and 4.18 show the average degree and average shortest path for RCL, respectively. The corresponding error is also shown for each data point. To calculate these parameters, we break our rectangular cuboid RCL sample to smaller rectangular cuboid boxes with same ratio between edges as the RCL sample. For each particular box size, the RCL is divided into as many number of boxes as possible without boxes overlapping. Then, the corresponding parameter is

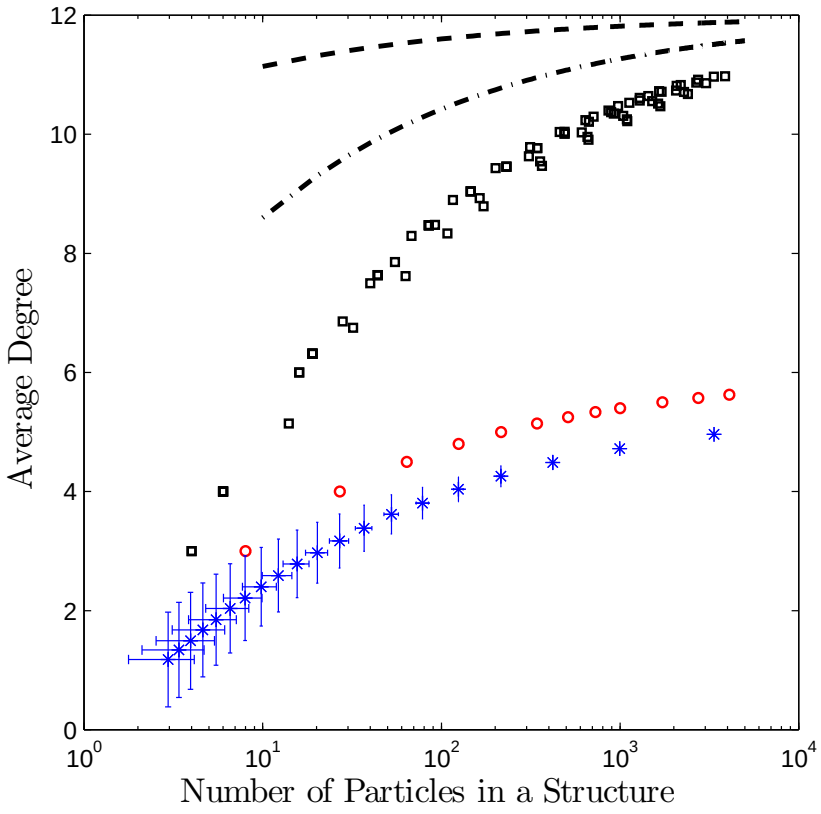

Figure 4.17: Network analysis of a reconstructed catalyst layer. Blue data shows the average degree of particles in the reconstructed catalyst layer and corresponding errors. The red and black markers show the average degree for a simple cubic and face centred cubic packing of same size spherical particles, respectively. The dashed and dotted-dashed lines show the upper bound of average degree for the general packing and face centred cubic packing, respectively.

calculated for each box, and the error bars are calculated as the mean square error of all boxes of a particular size. For example if the size of a box in each dimension is $\frac{1}{4}$ of the CL sample, the sample can be divided into 64 boxes.

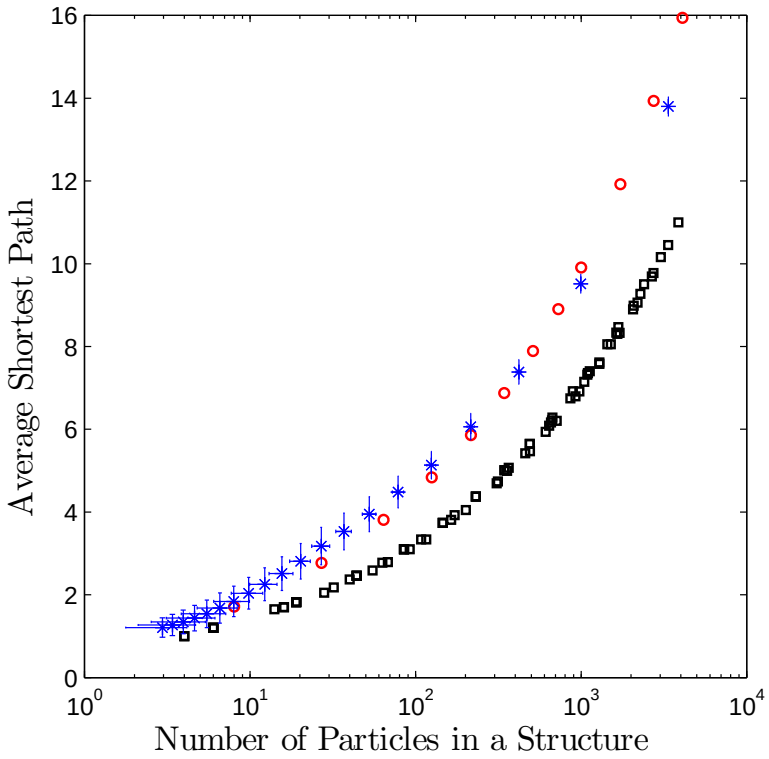

Figure 4.18: Network analysis of a reconstructed catalyst layer. Blue data shows the average shortest path of particles in the reconstructed catalyst layer and corresponding errors. The red and black markers show the average shortest path for a simple cubic and face centred cubic packing of same size spherical particles, respectively.

Each box contains a number of particles. First, an average number of particles for these 64 boxes is calculated, as well as a corresponding mean square error (i.e. horizontal error bars in Figures 4.17 and 4.18). Then, the desired network science parameter for each box is calculated, and again an average value and the corresponding mean square error are reported (i.e. vertical error bars in Figures 4.17 and 4.18).
When a box is defined, the connections between particles inside and outside the box are neglected, and then, the required parameters are calculated inside each box. As the size of the box changes, the average number of particles in the box changes too.

For comparison, we also plotted some other data. The red data with circle marker corresponds to a simple cubic (sc) packing of same size spherical particles. Similar to the previous part, we break the packing to cube boxes and calculate the parameters. Also, the data shown by square markers is for a face centred cubic (fcc) packing of spheres. The scatter in data is a result of how the packing is broken to smaller structures while the fcc packing is preserved.

The black dashed and dotted dashed lines in Figure 4.17 correspond to the upper bound of average degree for the general packing and face centred cubic (fcc) packing of spheres (Bezdek and Khan, 2016). One should note that these upper bounds are more relevant for high number of particles.

Figure 4.17 shows that for a simple cubic packing of spheres, the average degree is always higher than the RCL. This implies that a simple cubic packing forms a more compact structure compared to the RCL. In other words, this catalyst layer was fabricated under conditions that resulted in structures which are not as compact as a simple cubic packing. Thus, the agglomeration patterns that are formed during preparation of this CL contain particles that on average have less number of connections (or particles at contact) compared to a simple cubic packing.

However, as the number of particles increases, the average shortest path of simple cubic packing becomes higher than the RCL. The reason is the "degree distribution" of particles. In a simple cubic packing, there is no particle with a degree higher than 6. However, in the RCL, the degree of particles can be as high as 12. Particles (or nodes) with high degree can reduce the shortest path. Thus, although the average degree of the RCL is lower than the simple cubic packing, its average shortest path can become lower than the simple cubic packing.

On the other hand, the average degree for all particles inside a fcc packing

is 12, and only the particles in outer layer have lower degrees. That is why the average degree is lower than 12 at low particle numbers and it goes toward 12 as the particle number goes toward infinity (same argument is true for the average degree of 6 for a simple cubic packing). Since 12 is the highest degree for packing of the same size spherical particles ("Kissing number problem"), many of particles in fcc packing, indeed, have the highest possible degree. Thus, a fcc packing always has an average degree higher than our RCL sample, and its average shortest path is always lower than the RCL (see Figures 4.17 and 4.18).

Above discussion shows the importance of the degree distribution of a structure as a very fundamental concept, and also the importance of considering different network science concepts together for extracting more information from same data.

4.11 Summary

The motivation of this project was the need to improve fundamental understanding of the agglomeration and structure formation process that happens in colloidal suspensions, with a particular focus on suspensions similar to fuel cell catalyst layer inks. Agglomeration is a ubiquitous phenomenon, and understanding and controlling its process is important in a wide range of systems.

For fundamental phenomena such as agglomeration process that have been studied for a long time, achieving a new insight sometimes requires "seeing the problem through new eyes". We believe that implementing network science concepts to analyze the agglomeration process enabled us to do so.

The usefulness of network science has been shown in analyzing various complicated systems (Pastor-Satorras and Vespignani, 2001; Girvan and Newman, 2002; Rolland *et al.*, 2014). On the other hand, we showed that an agglomeration of particles can be appropriately modeled by a graph or network. We also showed that network science is a valuable tool to analyze a system of particles providing insights and improved understanding.

The power of network science depends on having the knowledge/information about some basic and fundamental characteristics of the system; for example in our case this is the position of each particle in our colloidal suspensions. While this basic information cannot be readily obtained experimentally, nu-

merical simulations enabled us to do so.

The novelty of this work lies in the novel implementation of a analysis tool (network science) to an old and ubiquitous problem (agglomeration process), and became possible with recent technological capabilities (computational/numerical capabilities). Our effort resulted in a new "perspective/insight" about the problem and improved our understanding: an "agglomeration timescale" and a "restructuring timescale" introduced to interpret the evolution of the agglomeration process suggest that the structure formation can be controlled by tuning the rate at which particles are added based on the restructuring timescale.

Chapter 5

Conclusion

In this work, we have studied the agglomeration process of particles in a colloidal suspension. An open source N-body code called *REBOUND* has been used as the numerical tool to simulate such systems. We have run simulations under various conditions, and gained new insights into fundamental reasons for differences between formed agglomerations.

In keeping with the practical motivations for this work, we have mainly focused on simulating colloidal suspensions that are similar to catalyst layer ink of PEM fuel cells. For more realistic simulations, the interaction between particles is defined using real physical potentials, rather than commonly used potential models. A comprehensive study about all relevant physical forces for such a system has been done. It has been shown that agglomeration patterns are directly related to the interaction force, thus assuming general potential models in simulations is not adequate.

To analyze the results of our simulations, a novel technique has been used. The formation and evolution of agglomerations are studied using network science concepts. This technique helped us to develop a new understanding about agglomeration process.

In this new understanding, we considered the full structure formation process as two steps: first, separated particles get together and form a structure, with a corresponding timescale that we call the "agglomeration timescale", t_{agg}. Second, the formed structures can restructure due to interaction between particles and evolve to a new structure if enough time is given. We call the corresponding timescale for this step the "restructuring timescale", t_{rest}. The full structure formation process depends on these two timescales, and corresponding available times for each step.

Overall, adding a new particle to a structure reduces the average number of connections between particles (the average degree) because the particle is usually added to outer layers of a structure where particles with lower number of connections are. A structure with lower average number of connections is a less compact structure. On the other hand, restructuring in systems with attractive forces increases the average number of connections between particles, which results in more compact structures. Thus, any change in the system that increases the rate of adding particles without reducing restructuring timescale correspondingly, results in less time for restructuring and makes structures less compact. So, the final structure of agglomerations can be controlled by tuning the rate of adding particles (t_{agg}) based on the restructuring timescale (t_{rest}) in the system.

To expand on this work, one can apply the same network science analysis on structures of different sizes in the system, rather than largest structures that were considered in this work. Since agglomeration is a dynamic process, the state of the system changes as agglomeration continues, and the remaining free particles agglomerate in patterns that can be different than the primary formed structures. This can improve our understanding on how to tune various parameters to form desired structures.

As noted in the previous chapters, the polymer phase is not resolved in this study. Preliminary simulations of nanoparticules agglomeration where different ratio of particles were assumed to be charged on the surface with similar order of magnitude to electrostatic interaction if they were covered by polymer in CL ink (i.e beside the attractive interaction force between all particles, a repulsive electrostatic force was also defined between some of the particles), have indicated that some of the charged particles were present inside the agglomerations. Although this is a simplified representation that does not explicitly resolve the polymer phase (e.g. other related forces such as polymer related steric repulsive force were not accounted for), the preliminary results are consistent with some of the new findings of penetration of polymer into carbon agglomerations in catalyst layer inks. Future works could investigate this more comprehensively.

Another interesting question is to investigate the effect of Brownian motion on agglomeration patterns. In colloidal systems with small particles, the Brownian motion of particles can change their movement direction. How significant it can be compared to interaction between particles when particles are in the vicinity of each other, and how it can change the agglomeration patterns is yet to be studied.

The usefulness of network science as an analysis tool, previously demonstrated in other disciplines, has also been shown in this work by analyzing the agglomeration process and characterizing the agglomeration patterns. Considering various concepts together can provide new insights and a better understanding of the problem studied. Some examples (considering various parameters such as degree, shortest path, degree distribution, etc. together) were presented in this work, while other concepts such as weighted degree (that defines the degree based on the actual distance between particles) or clustering coefficient (which counts triplet connections in a structure) will be discussed in future studies.

Catalyst layer is considered as a homogeneous and isotropic porous medium. Thus, theories such as "percolation theory" (Isichenko, 1992; Saberi, 2015), (which describes the behavior of a system that can be represented as a random graph) can be useful in studying various properties of the catalyst layer (and also other parts of a fuel cell), for example in describing transport properties, electron and ion conductivity, or investigating material characteristics (Secanell *et al.*, 2008; Chen *et al.*, 2009; Devanathan *et al.*, 2010; Wu *et al.*, 2011; Synodis *et al.*, 2013; Alink and Gerteisen, 2013).

On the other hand, after conducting this study that focuses on the catalyst layer ink (where agglomerates that are building blocks of the final solid catalyst layer are formed), we believe that not only the agglomeration patterns and formed structures can be characterized by network science concepts, but also the process itself can be better understood if the system of colloidal suspension is considered as a "*complex network*"; that is a network/graph which is neither completely regular nor completely random, and thus can have non-trivial features that are not present in simple networks such as lattice or random graphs. This suggests that in future studies, appropriate concepts (such as weighted degree defined based on the actual distance between particles) can be considered to describe the system from the beginning when all particles are dispersed. Thus, the agglomeration process can be studied even before agglomerates are formed. While detailed analysis and advanced graph theory and statistical calculations will be required to interpret the data, we believe this approach can offer further fundamental understanding of the agglomeration process.

Finally, the physical representation of the system can be further improved using CFD simulations that resolve hydrodynamic interactions. However such simulations are computationally intensive and are not yet practical for physically representative systems comprising a sufficient number of particles.

Again, the novel application of network science presented in this work has illustrated the usefulness of this powerful analysis tool and provided new insights about the agglomeration process, explaining and predicting this phenomenon in a much deeper manner than before.

Appendices

Appendix A

Fuel Cell Catalysts Ink

This appendix describes the preparation of catalyst layer ink. Although this thesis focuses on theoretical modelling, a good understanding of the physical ink preparation process is important on several levels. First, we need to identify and quantify the physical parameters to simulate the agglomeration process in a colloidal suspension relevant to a catalyst layer ink. It is therefore useful to review the ink preparation techniques, used materials, and various recipes whether all the details are included in simulations or not. The ink components and their characteristics are also important to select the appropriate interaction potentials between the particles in our simulations. Also, the simulations undertaken in this work require a number of assumptions that need to be justified on light of the ink preparation techniques (for example see A.3.2).

A.1 Ink Preparation for PEM Fuel Cell Catalyst Layer Fabrication

In the following, some information related to materials (such as type or size of particles etc.) and procedures (such as stirring or sonication rate and time etc.) are summarized with the corresponding references.

A.2 Material

A.2.1 Pt/C Particles

CL is the heart of the fuel cell since the electrochemical reactions occur there. These reactions happen with the help of a catalyst which is usually Platinum (Pt) in proton exchange membrane (PEM) fuel cells. The Pt particles are supported by carbonaceous substrates which also assure the electron conductivity to the Pt reaction sites. The most common carbon supports are Vulcan XC-72 and Ketjen Black (Soboleva *et al.*, 2010). These carbon supports are considered as very high conducting carbon blacks, although over mixing and/or processing can significantly decrease their electron conductivity. Carbon black particles are intensely black, finely divided form of amorphous carbon, and are usually spherical in shape.

The size of the Pt nanoparticles range from $2-5$ nm (Malek *et al.*, 2007; Cheng *et al.*, 2010; Takahashi and Kocha, 2010; Xiao *et al.*, 2012), while the Vulcan XC-72 carbon particles have a diameter of $20-30$ nm (Malek *et al.*, 2007; Xiao *et al.*, 2012). The size of Vulcan XC-72 particles can also be in the range of $30-60$ nm (Chai *et al.*, 2004). The average size of Ketjen black carbon particle is around 39.5 nm (Iwata *et al.*, 2007). Also, the average size of some other supports such as Prentex XE-2, Vulcan XC-72R, Acetylene Black, and Black Pearls 2000 are 30 nm, 30 nm, 35 nm, and less than 30 nm, respectively (Iwata *et al.*, 2007).

The ratio of Pt to carbon in Pt/C powders is usually reported in weight percent, and it varies in a range of a few to a few tens wt.% based on the various required CL performances. The Pt to carbon support weight ratio is the ratio of weight of Pt to the weight of the carbon support (Litster and McLean, 2004). (However, it seems the correct definition for the weight ratio is the weight of Pt to the total weight of Pt + C.)

A.2.2 Solvent

Some of the typical solvents used in CL ink are: ethylene glycol ($\varepsilon = 37.7$, where ε is the dielectric constant), isopropyl alcohol ($\varepsilon = 18.3$), and hexane ($\varepsilon = 1.9$). Also, water has a dielectric constant of around 80. One of the reasons to use another solvent in addition to water is to make a good dispersion; some types of catalyst alloys and/or carbon supports are inherently hydrophobic which makes it difficult to wet them with only water and make

a good dispersion (Garsany *et al.*, 2010; Takahashi and Kocha, 2010).

Dielectric constant of the solvent changes the state of the Nafion ionomer in the ink solution. For solvents with dielectric constant > 10, Nafion forms a solution, while it forms a colloid for solvents with dielectric constant between 3 and 10, and a precipitate for solvents with dielectric constant < 3. The typical solvent to form a solution state is ethanol ($\varepsilon = 24.3$) or isopropyl alcohol, while butyl acetate ($\varepsilon = 5.01$) is the typical solvent to form a colloidal state (Shin *et al.*, 2002; Zhang, 2008).

Moreover, the interaction between solvent, Nafion, and Pt/C particles results in different agglomerate sizes in various solvent media (Xu *et al.*, 2010). For example, due to the formation of larger agglomerates, colloidal method is preferred for the spraying technique (Shin *et al.*, 2002).

A better performance at high current densities has been observed for cells prepared by colloidal method compared to the solution method. This can be explained as a result of higher mass transport due to higher porosity formed by larger agglomerates, as well as higher proton conductivity due to the continuous network of ionomer in colloidal method (Litster and McLean, 2004).

A.2.3 Nafion Solution

Nafion is a synthetic polymer with ionic properties which is called ionomer. Ionomers are conductive to ions but not electrons. Because of this feature, as well as the good thermal and mechanical stability, Nafion has been used extensively as the proton conductor membrane in PEM fuel cells. Nafion chemical formula is $C_7HF_{13}O_5S \ . \ C_2F_4$ (a sulfonated tetrafluoroethylene based fluoropolymer-copolymer), and in a dilute solution, it can be considered as a rodlike particle with a length of $\sim 20 - 30$ nm and a diameter of $2 - 3$ nm (Loppinet *et al.*, 1997; Gebel, 2000; Xu *et al.*, 2010)

While Nafion films are used as the membrane in PEM fuel cells, Nafion solution is also added to the CL ink to assure protonic conduction to the reaction sites in the CL, as well as bonding Pt/C particles together in the solid CL. A typical Nafion solution is a 5 wt.% solution in a mixture of water and lower aliphatic alcohols (Martin *et al.*, 2010). Some of the commonly used commercial Nafion solutions are as following (SIGMA-ALDRICH website - www.sigmaaldrich.com):
Nafion perfluorinated resin solution - 5 wt.% in mixture of lower aliphatic alcohols and water, contains 45 % water (Product Number: 510211): This

product contains 45 wt.% water ($42.0 - 48.0$ wt.%), $45.0 - 51.0$ wt.% 1-Propanol, less than 4.0 wt.% Ethanol, less than 1.0 wt.% miscellaneous, and a solid content of $5.0 - 5.4$ wt.%. At 25 °C, its density is 0.921 g/mL.
Nafion perfluorinated resin solution - 5 wt.% in lower aliphatic alcohols and water, contains $15 - 20$% water (Product Number: 274704): This product contains approximately $15 - 25$% water, $16 - 30$% n-Propanol, $15 - 30$% 2-Propanol, less than 5% Polyoxyethylene ethers, with a residue on evaporation of $4 - 6$%. At 25 °C, its density is 0.874 g/mL .

Curtin *et al.* (2004) did some measurements on viscosity and surface tension of Nafion polymer dispersion (Nafion solution is also called Nafion dispersion). For nominal 10% solids aqueous dispersions, they found typical viscosities of between 4 and 5 cP (centipoise) at 40 s^{-1} shear rate and a temperature of 25 °C (At high temperatures of around 250 °C, the viscosity of the aqueous dispersion reduced to approximately 2 cP). For comparison, the viscosity of water is 1.79 cP, 1.14 cP, 1 cP, 0.89 cP, 0.8 cP, and 0.66 cP at 0 °C, 15 °C, 20 °C, 25 °C, 30 °C, and 40 °C, respectively, and the viscosity of isopropyl alcohol is 4.56 cP, 2.86 cP, 2.37 cP, 1.96 cP, 1.77 cP, and 1.33 cP at 0 °C, 15 °C, 20 °C, 25 °C, 30 °C, and 40 °C, respectively. Curtin *et al.* (2004) also reported a surface tension of 25 mNm^{-1} for a polymer dispersion containing 20% polymer, 34% water and 46% 1-propanol. For a dispersion of 5% polymer, 45% water, and 50% alcohol, their work suggests a surface tension of ~ 30 mNm^{-1}.

A.3 Procedure

A.3.1 Material Ratio

To form an efficient electrode, the optimum ratio of ionomer (dry Nafion) to carbon is found to be $\sim 0.8 - 1$ by weight (Zhang, 2008; Xiao *et al.*, 2012). Also, a typical weight ratio to make a hydrophilic ink (Pt/C particles, Nafion solution, and water/glycerol as the solvent) is about $1 : 5 : 20$ for carbon/water/glycerol, respectively (Litster and McLean, 2004; Zhang, 2008).

Moreover, one example of the commonly used ink formulation in the industry is reported by Xie *et al.* (2008) as follows:
Alcohol-based ink (also called Ink-p): Solid content 1 wt.%, n-Propanol 77 wt.%, Water 22 wt.%

There is also water-based ink (Ink-w) with the following formulation (Xie *et al.*, 2008):
Water-based ink: Solid content 1 wt.%, n-Propanol 3 wt.%, Water 96 wt.%. The small amount of n-Propanol in water-based ink is due to presence of n-Propanol in Nafion solution. To make the CL, Xie *et al.* (2008) used Pt/C powder of 46.5 wt.% Pt (TEC10E50E, Tanaka Kikinzoku Kogyo) (0.40 mg cm^{-2} Pt), and their dried CL contained 30 wt.% Nafion ionomer (To make the CL ink, they used the 5 wt% Nafion solution, EW1000, Alfa Aeser).

One of the optimal ink formulation reported by Takahashi and Kocha (2010) is as following:
18.5 mg of (46 wt.% Pt/C) TEC10E50E is mixed with 19 mL of DI water and 6 mL of isopropyl alcohol. This mixture, along with 100 μL of 5% Nafion solution are added to a 50 mL sample bottle. The sample bottle is ultrasonicated for 30 min in a small ice bath, and the ink is ready for deposition (10 μL, 17.3 $\mu gPtcm^{-2}$).

Takahashi and Kocha (2010) also systematically changed the ratio of isopropyl alcohol and water, and found that the optimum volume ratio of isopropyl alcohol/total volume is around 35% to maximize the electrochemical area.

Garsany *et al.* (2010) also suggested two recipes to make a thin-film electrode as following:
The first recipe uses 20% Pt on Vulcan carbon to make an electrode with a Pt loading of 20 $\mu gPtcm^{-2}$. 20 mL of isopropyl alcohol is mixed with 79.6 mL of nanopure water and 0.4 mL of 5 wt.% Nafion ionomer solution (Ion Power, Liquion 1100) to make a solution of 20% isopropyl alcohol and 0.02% Nafion ionomer. 5 mL of this solution is added to 10 mg of Pt/C powder (20% Pt on Vulcan carbon), and the mixture is mixed thoroughly with a high shear mixer (IKA, T10Basic S1). The ink is then sonicated for ≥ 60 min in a water bath with temperature $< 40\,^{\circ}C$ using a Branson 2510 ultrasonicator. The second recipe uses 46% Pt on Ketjen black to make an electrode with a Pt loading of 17.3 $\mu gPtcm^{-2}$. 6 mL of isopropyl alcohol is mixed with 19 mL of nanopure water to make a 24% isopropyl alcohol solution. 25 mL of this solution is added to 18.5 mg of Pt/C powder (46% Pt on Ketjen black), and finally, 100 μL of 5 wt.% Nafion ionomer solution (Ion Power, Liquion 1100) is added to the Pt/Ketjen black/isopropyl alcohol solution. The final mixture is then sonicated for 30 min in an ice bath using a Branson 2510 ultrasonicator.

Pollet and Goh (2014) used the following formula to make their ink:

They used 5 mg of the commercial Pt/C catalyst, and added 5.14 mL of ultrapure water, 28 μL of Nafion solution (10 wt.%, EW1100, D1021, DuPont), and 1.62 mL of isopropyl alcohol to make their ink sample ($V = 7$ mL). This mixture was hand-shaken vigorously for 5 min, followed immediately by ultrasonication (See sonication section for the details of their sonication procedure).

It is clear from the above trail and error variations in "recipes" that a better understanding of ink formation is required to improve and optimise ink preparation and CL fabrication.

A.3.2 Sonication/Stirring

Sonication is the irradiation of a sample with sound wave/energy resulting in the agitation of particles in the sample for various purposes. When the ultrasonic frequencies are used, the process is also called ultrasonication. The frequency range of ultrasound is usually defined as the above 16 kHz with an upper limit of 5 MHz for gases and 500 MHz for liquids and solids (Pollet, 2010). There are two main types of ultrasonication: low frequency or power ultrasound (20−100 kHz), and high frequency or diagnostic ultrasound (2−10 MHz).

Over the past few years, power (low frequency) ultrasonication has been widely used in the fabrication of fuel cell materials; preparing noble metal electrocatalysts, carbon support electrocatalysts, and fuel cell electrolyte materials (Pollet, 2010). Moreover, sonication has also been used as the mixing method during the fabrication of the CL ink, although the effect of sonication on ink preparation has not been studied comprehensively. The typical ultrasonic frequency used during ink mixing procedure is 20 kHz when using an ultrasonic probe, or $38 - 40$ kHz when using an ultrasonic bath (Pollet and Goh, 2014).

There is no universal defined procedure of sonication during ink preparation. Recently, Pollet and Goh (2014) did a study on the importance of the ultrasonic parameters in the CL ink preparation. Based on their results, they suggested that ultrasonic equipment, frequencies, powers and durations should be reported in the works that use ultrasound treatment, since each of these factors can change the final results.

A typical duration of sonication is around a few minutes to half an hour after adding water/solvent to Pt/C powder (this step is skipped by some groups), and half an hour to two hours of sonication after adding Nafion

solution to Pt/C and water/solvent mixture (Garsany *et al.*, 2010; Martin *et al.*, 2010; Soboleva *et al.*, 2010; Xu *et al.*, 2010; Xiao *et al.*, 2012)

However, Takahashi and Kocha (2010) reported that a sonication of $10 - 15$ min (after adding all the ink's components) is sufficient to make a good dispersion. They did not observe any significant change after sonication of their samples for longer than 15 min up to a period of 3 h, which suggests a strong adhesion of Pt to the carbon support. They also argued that a period of 5 min of sonication was not enough to make reproducible samples. Takahashi and Kocha (2010) used TEC10E50E ($\sim$ 46 wt.% Pt/C), TEC10E50-HT ($\sim$ 46 wt.% Pt/C-heat treated (HT)), as well as an alloy catalyst TEC36E52 ($\sim$ 46 wt.% PtCo/C) in their study.

On the other hand, Pollet and Goh (2014) showed that ultrasonication for longer periods and at high powers can have negative effects on ink composition, as a result of cavitation and sonolysis phenomena. They used two commercial carbon supported Pt catalysts (Pt/C, C: Vulcan XC-72R), Tanaka Kikinzoku Kogyo (TEC10E50E; 45.9 wt.% Pt/C TKK, Japan) and E-TEK (HP $\sim$50 wt.% Pt/C, USA) to make their ink samples. They also ultrasonicated their samples (at a temperature of 298 ± 1 K) for various durations ($t = 0, 10, 30, 60$ and 120 min) either using an ultrasonic probe with frequency of 20 kHz (20 kHz Vibra-Cell VCX750 with a tip diameter of 6 mm - Sonics & Materials Inc.) and a power of up to 12.23 W (3.03 W, 6.70 W, 12.23 W) or an ultrasonic bath with a frequency of 40 kHz (40 kHz Ultrasonic 375H - Langford Electronics Ltd.,Coventry, UK) and a power of 1.82 W. To make a sample ($V = 7$ mL), they used 5 mg of the commercial Pt/C catalyst, and added 5.14 mL of ultrapure water, 28 μL of Nafion solution (10 wt.%, EW1100, D1021, DuPont), and 1.62 mL of isopropyl alcohol. This mixture was hand-shaken vigorously for 5 min, followed immediately by ultrasonication.

Pollet and Goh (2014) found that for the ink samples prepared using E-TEK catalysts, ultrasonic bath (40 kHz, 1.82 W) results in higher electrochemical surface area (ECSA) than ultrasonic probe (20 kHz, $3.03 - 12.23$ W). A maximum ECSA was achieved after 30 min of ultrasonication using ultrasonic bath and ultrasonic probe at the two lower ultrasonic powers (3.03 W and 6.7 W). Their results also suggest that the ECSA of samples sonicated for 120 min are $10 - 15\%$ lower than ECSA values after 30 min sonication. Moreover, they observed a significant decrease in ECSA as the ultrasonic power increases.

For ink samples prepared using TKK catalysts, Pollet and Goh (2014)

found that on average, ultrasonication using ultrasonic bath results in considerably lower ECSAs than ultrasonic probe. Also, while the E-TEK samples required at least 30 min of ultrasonication in order to form reproducible results, 10 min of ultrasonication found to be enough to form reproducible TKK samples prepared by ultrasonic probe. For TKK samples prepared by ultrasonic bath, a period of at least 30 min of ultrasonication is still needed. Similar to the E-TEK samples, they found that the ECSA decreases as the ultrasonication time increases. However, the decrease in TKK samples was typically $< 10\%$ compared with $10 - 15\%$ for E-TEK samples under similar conditions. This implies that the TKK catalyst is more resistant to cavitation effects of sonication, which suggests a stronger adhesion of Pt particles on the carbon support for the TKK catalyst compared to E-TEK. Also, similar to E-TEK samples, high ultrasonic powers resulted in lower ECSA values than low ultrasonic powers using the ultrasonic probe.

Based on the range of parameters considered in their work, Pollet and Goh (2014) suggested the optimum operating powers of 1.82 W and 3.03 W when using an ultrasonic bath and ultrasonic probe devices, respectively.

For the purpose of comparison between studies, Pollet and Goh (2014) also made some of their samples using a high-shear mixer (Heidolph Silent Crusher) operating at 19000 rpm with a rotor diameter of 3.2 mm (no ultrasonic treatment was done for these samples). The mixing of CL ink samples ($V = 7$ mL) was done for various durations ($t = 0, 10, 30, 60$ and 120 min) at a temperature of 298 ± 1 K. They found that the ECSA values for samples treated by high-shear mixing were considerably lower than ultrasonicated samples. Also, high-shear mixing did not result in any dislodgement of Pt nanoparticles from the carbon support. Moreover, larger agglomerates were observed in samples prepared by high-shear mixer. Pollet and Goh (2014) also reported that a 60 min of high-shear mixing was required to achieve the maximum ECSA.

The few studies about sonication of CL ink were mainly focused on the effect of sonication on Pt nanoparticles. However, the sonication effect on agglomeration of carbon particles also merits more attention since it can considerably change the CL structure, affecting the fuel cell performance. Numerical simulations on particles agglomeration which also model sonication treatment can be a useful tool for studying the effect of sonication on carbon particles agglomeration.

In this work, we do not model the sonication process in our simulations. Indeed, the beginning of our simulations correspond to the end of the sonica-

tion step. The goal of sonication is to ensure that all the agglomerates in the suspension (that were formed before or during adding carbon nanoparticles to the suspension) are broken down, and carbon nanoparticles are uniformly distributed in the suspension, so the new structures in the ink are formed from the smallest carbon nanoparticles that are well mixed in the system. In our simulations, we capture this point by randomly distributing the carbon particles in our simulation's domain, and starting the simulation from this state.

Bibliography

Adams, J. E. and Stratt, R. M. (1990) Instantaneous normal mode analysis as a probe of cluster dynamics. *The Journal of Chemical Physics* **93**(2), 1332–1346.

Albert, R. and Barabási, A.-L. (2002) Statistical mechanics of complex networks. *Rev. Mod. Phys.* **74**, 47–97.

Alink, R. and Gerteisen, D. (2013) Modeling the liquid water transport in the gas diffusion layer for polymer electrolyte membrane fuel cells using a water path network. *Energies* **6**(9), 4508–4530.

Asakura, S. and Oosawa, F. (1954) On interaction between two bodies immersed in a solution of macromolecules. *Chemical Physics* (22), 1255–1256.

Asakura, S. and Oosawa, F. (1958) Interaction between particles suspended in solutions of macromolecules. *Journal of polymer science* **33**(126), 183–192.

Attard, P. (1989) Long-range attraction between hydrophobic surfaces. *The Journal of Physical Chemistry* **93**(17), 6441–6444.

Barabási, A.-L. and Albert, R. (1999) Emergence of scaling in random networks. *Science* **286**(5439), 509–512.

Baroody, H. A., Stolar, D. B. and Eikerling, M. H. (2018) Modelling-based data treatment and analytics of catalyst degradation in polymer electrolyte fuel cells. *Electrochimica Acta* **283**, 1006 – 1016.

Baschuk, J. and Li, X. (2001) Carbon monoxide poisoning of proton exchange membrane fuel cells. *International Journal of Energy Research* **25**(8), 695–713.

Becker, V. and Briesen, H. (2010) A master curve for the onset of shear induced restructuring of fractal colloidal aggregates. *Journal of Colloid and interface Science* **346**(1), 32–36.

Becker, V., Schlauch, E., Behr, M. and Briesen, H. (2009) Restructuring of colloidal aggregates in shear flows and limitations of the free-draining approximation. *Journal of colloid and interface science* **339**(2), 362–372.

Bezdek, K. and Khan, M. A. (2016) Contact numbers for sphere packings. *arXiv preprint arXiv:1601.00145* .

Bonin, K. D. (1997) *Electric-Dipole Polarizabilities of Atoms, Molecules, And Clusters*. Wspc.

Born, G. V. R. (1962) Aggregation of blood platelets by adenosine diphosphate and its reversal. *Nature* **194**(4832), 927–929.

Borup, R., Meyers, J., Pivovar, B., Kim, Y. S., Mukundan, R., Garland, N., Myers, D., Wilson, M., Garzon, F., Wood, D. *et al.* (2007) Scientific aspects of polymer electrolyte fuel cell durability and degradation. *Chemical reviews* **107**(10), 3904–3951.

Brasil, A., Farias, T. L. and Carvalho, M. (1999) A recipe for image characterization of fractal-like aggregates. *Journal of Aerosol Science* **30**(10), 1379–1389.

Butt, H., Graf, K. and Kappl, M. (2006) *Physics and Chemistry of Interfaces*. Wiley.

Cetinbas, F. C., Ahluwalia, R. K., Kariuki, N. N. and Myers, D. J. (2018) Agglomerates in polymer electrolyte fuel cell electrodes: Part i. structural characterization. *Journal of The Electrochemical Society* **165**(13), F1051–F1058.

Chai, G. S., Yoon, S. B., Yu, J.-S., Choi, J.-H. and Sung, Y.-E. (2004) Ordered porous carbons with tunable pore sizes as catalyst supports in direct methanol fuel cell. *The Journal of Physical Chemistry B* **108**(22), 7074–7079.

Chen, D., Lin, Z., Zhu, H. and Kee, R. J. (2009) Percolation theory to predict effective properties of solid oxide fuel-cell composite electrodes. *Journal of Power Sources* **191**(2), 240–252.

Cheng, C., Malek, K., Sui, P. and Djilali, N. (2010) Effect of pt nano-particle size on the microstructure of pem fuel cell catalyst layers: Insights from molecular dynamics simulations. *Electrochimica Acta* **55**(5), 1588–1597.

Cherevko, S., Kulyk, N. and Mayrhofer, K. J. (2016) Durability of platinum-based fuel cell electrocatalysts: Dissolution of bulk and nanoscale platinum. *Nano Energy* **29**, 275 – 298. Electrocatalysis.

Choi, Y. J. and Djilali, N. (2016) Direct numerical simulations of agglomeration of circular colloidal particles in two-dimensional shear flow. *Physics of Fluids* **28**(1), 013304.

Christenson, H. K. and Claesson, P. M. (1988) Cavitation and the interaction between macroscopic hydrophobic surfaces. *Science* **239**(4838), 390–392.

Claesson, P. M. and Christenson, H. K. (1988) Very long range attractive forces between uncharged hydrocarbon and fluorocarbon surfaces in water. *The Journal of Physical Chemistry* **92**(6), 1650–1655.

Clauset, A., Newman, M. E. J. and Moore, C. (2004) Finding community structure in very large networks. *Phys. Rev. E* **70**, 066111.

Craig, V. S., Ninham, B. W. and Pashley, R. M. (1993) The effect of electrolytes on bubble coalescence in water. *The Journal of Physical Chemistry* **97**(39), 10192–10197.

Curtin, D. E., Lousenberg, R. D., Henry, T. J., Tangeman, P. C. and Tisack, M. E. (2004) Advanced materials for improved {PEMFC} performance and life. *Journal of Power Sources* **131**(12), 41 – 48.

Danckwerts, P. V. (1952) The definition and measurement of some characteristics of mixtures. *Applied Scientific Research, Section A* **3**(4), 279–296.

de Paula Peter Atkins, J. (2010) *Physical Chemistry for the Life Sciences*. Oxford University Press.

De Temmerman, P.-J., Van Doren, E., Verleysen, E., Van der Stede, Y., Francisco, M. A. D. and Mast, J. (2012) Quantitative characterization of agglomerates and aggregates of pyrogenic and precipitated amorphous silica nanomaterials by transmission electron microscopy. *Journal of Nanobiotechnology* **10**(1), 24.

Derjaguin, B. V. (1934) Untersuchungen über die reibung und adhäsion, iv. *Colloid & Polymer Science* **69**(2), 155–164.

Devanathan, R., Venkatnathan, A., Rousseau, R., Dupuis, M., Frigato, T., Gu, W. and Helms, V. (2010) Atomistic simulation of water percolation and proton hopping in nafion fuel cell membrane. *The Journal of Physical Chemistry B* **114**(43), 13681–13690.

Djilali, N. (2007) Computational modelling of polymer electrolyte membrane (pem) fuel cells: Challenges and opportunities. *Energy* **32**(4), 269 – 280. ECOS 05. 18th International Conference on Efficiency, Cost, Optimization, Simulation, and Environmental Impact of Energy Systems.

Donaldson Jr, S. H., Røyne, A., Kristiansen, K., Rapp, M. V., Das, S., Gebbie, M. A., Lee, D. W., Stock, P., Valtiner, M. and Israelachvili, J. (2014) Developing a general interaction potential for hydrophobic and hydrophilic interactions. *Langmuir* **31**(7), 2051–2064.

Drobny, J. (2011) *Polymers for Electricity and Electronics: Materials, Properties, and Applications*. Wiley.

Eberle, U., Müller, B. and Von Helmolt, R. (2012) Fuel cell electric vehicles and hydrogen infrastructure: status 2012. *Energy & Environmental Science* **5**(10), 8780–8798.

Eggersdorfer, M., Kadau, D., Herrmann, H. J. and Pratsinis, S. E. (2010) Fragmentation and restructuring of soft-agglomerates under shear. *Journal of colloid and interface science* **342**(2), 261–268.

Everhart, E. (1985) An efficient integrator that uses gauss-radau spacings. In *International Astronomical Union Colloquium*, volume 83, pp. 185–202. Cambridge University Press.

Garsany, Y., Baturina, O. A., Swider-Lyons, K. E. and Kocha, S. S. (2010) Experimental methods for quantifying the activity of platinum electrocatalysts for the oxygen reduction reaction. *Analytical Chemistry* **82**(15), 6321–6328.

Gebel, G. (2000) Structural evolution of water swollen perfluorosulfonated ionomers from dry membrane to solution. *Polymer* **41**(15), 5829 – 5838.

Girvan, M. and Newman, M. E. J. (2002) Community structure in social and biological networks. *Proceedings of the National Academy of Sciences* **99**(12), 7821–7826.

Goldburg, W. (1999) Dynamic light scattering. *American Journal of Physics* **67**(12), 1152–1160.

Grahame, D. C. (1953) Diffuse double layer theory for electrolytes of unsymmetrical valence types. *The Journal of Chemical Physics* **21**(6), 1054–1060.

Gröger, O., Gasteiger, H. A. and Suchsland, J.-P. (2015) Electromobility: Batteries or fuel cells? *Journal of The Electrochemical Society* **162**(14), A2605–A2622.

Hagan, M. F., Elrad, O. M. and Jack, R. L. (2011) Mechanisms of kinetic trapping in self-assembly and phase transformation. *The Journal of chemical physics* **135**(10), 104115.

Hamaker, H. (1937) The londonvan der waals attraction between spherical particles. *Physica* **4**(10), 1058 – 1072.

Henderson, D., Duh, D.-M., Chu, X. and Wasan, D. (1997) An expression for the dispersion force between colloidal particles. *Journal of Colloid and Interface Science* **185**(1), 265–268.

Higashitani, K. and Iimura, K. (1998) Two-dimensional simulation of the breakup process of aggregates in shear and elongational flows. *Journal of colloid and interface science* **204**(2), 320–327.

Hu, J., Sui, P., Kumar, S. and Djilali, N. (2009) Modelling and simulations of carbon corrosion during operation of a polymer electrolyte membrane fuel cell. *Electrochimica Acta* **54**(23), 5583–5592.

Hua, Q.-X., Gozani, S. N., Chance, R. E., Hoffmann, J. A., Frank, B. H. and Weiss, M. A. (1995) Structure of a protein in a kinetic trap. *Nature structural biology* **2**(2), 129.

Huya-Kouadio, J. (2017) Doe hydrogen and fuel cells program record .

Isichenko, M. B. (1992) Percolation, statistical topography, and transport in random media. *Reviews of modern physics* **64**(4), 961.

Israelachvili, J. and Pashley, R. (1982) The hydrophobic interaction is long range, decaying exponentially with distance .

Israelachvili, J. and Pashley, R. (1984) Measurement of the hydrophobic interaction between two hydrophobic surfaces in aqueous electrolyte solutions. *Journal of Colloid and Interface Science* **98**(2), 500–514.

Israelachvili, J. N. (2010) *Intermolecular and Surface Forces, Third Edition*. Academic Press, third edition.

Iwata, N., Yuasa, M., Oyaizu, K., Tanaka, K., Igo, Y., Yamamoto, M., Sasaki, S. and Kido, S. (2007) Process for preparing catalyst material. WO Patent App. PCT/JP2007/055,315.

Kukukova, A., Aubin, J. and Kresta, S. M. (2009) A new definition of mixing and segregation: Three dimensions of a key process variable. *Chemical Engineering Research and Design* **87**(4), 633 – 647. 13th European Conference on Mixing: New developments towards more efficient and sustainable operations.

Kusano, T., Hiroi, T. and Amemiya, K. (2015) Structural evolution of a catalyst ink for fuel cells during the drying process investigated by cv-sans. *Polymer Journal* **47**(8), 546–555.

Lange, K. J., Carlsson, H., Stewart, I., Sui, P.-C., Herring, R. and Djilali, N. (2012) Pem fuel cell cl characterization using a standalone fib and sem: Experiments and simulation. *Electrochimica Acta* **85**, 322–331.

Li, H., Tang, Y., Wang, Z., Shi, Z., Wu, S., Song, D., Zhang, J., Fatih, K., Zhang, J., Wang, H., Liu, Z., Abouatallah, R. and Mazza, A. (2008) A review of water flooding issues in the proton exchange membrane fuel cell. *Journal of Power Sources* **178**(1), 103 – 117.

Li, Q., He, R., Gao, J.-A., Jensen, J. O. and Bjerrum, N. J. (2003) The co poisoning effect in pemfcs operational at temperatures up to 200 c. *Journal of the Electrochemical Society* **150**(12), A1599–A1605.

Lifshitz, E. (1956) The theory of molecular attractive forces between solids. *Sov.Phys.JETP* **2**, 73–83.

Likos, C., Vaynberg, K., Löwen, H. and Wagner, N. (2000) Colloidal stabilization by adsorbed gelatin. *Langmuir* **16**(9), 4100–4108.

Limbach, L. K., Li, Y., Grass, R. N., Brunner, T. J., Hintermann, M. A., Muller, M., Gunther, D. and Stark, W. J. (2005) Oxide nanoparticle uptake in human lung fibroblasts: effects of particle size, agglomeration, and diffusion at low concentrations. *Environmental science & technology* **39**(23), 9370–9376.

Litster, S. and Djilali, N. (2005) Two-phase transport in porous gas diffusion electrodes. *Developments in Heat Transfer* **19**, 175.

Litster, S. and McLean, G. (2004) {PEM} fuel cell electrodes. *Journal of Power Sources* **130**(12), 61 – 76.

London, F. (1937) The general theory of molecular forces. *Trans. Faraday Soc.* **33**, 8b–26.

Loppinet, B., Gebel, G. and Williams, C. E. (1997) Small-angle scattering study of perfluorosulfonated ionomer solutions. *The Journal of Physical Chemistry B* **101**(10), 1884–1892.

Malek, K., Eikerling, M., Wang, Q., Navessin, T. and Liu, Z. (2007) Self-organization in catalyst layers of polymer electrolyte fuel cells. *The Journal of Physical Chemistry C* **111**(36), 13627–13634.

Mao, Y., Cates, M. and Lekkerkerker, H. (1995) Depletion force in colloidal systems. *Physica A: Statistical Mechanics and its Applications* **222**(1), 10–24.

Martin, S., Garcia-Ybarra, P. and Castillo, J. (2010) Electrospray deposition of catalyst layers with ultra-low pt loadings for {PEM} fuel cells cathodes. *Journal of Power Sources* **195**(9), 2443 – 2449.

McLachlan, A. D. (1963a) Retarded Dispersion Forces Between Molecules. *Royal Society of London Proceedings Series A* **271**, 387–401.

McLachlan, A. D. (1963b) Retarded dispersion forces in dielectrics at finite temperatures. *Proceedings of the Royal Society of London. Series A. Mathematical and Physical Sciences* **274**(1356), 80–90.

McLachlan, A. D. (1965) Effect of the medium on dispersion forces in liquids. *Discuss. Faraday Soc.* **40**, 239–245.

Meier, J. C., Galeano, C., Katsounaros, I., Witte, J., Bongard, H. J., Topalov, A. A., Baldizzone, C., Mezzavilla, S., Schüth, F. and Mayrhofer, K. J. (2014) Design criteria for stable pt/c fuel cell catalysts. *Beilstein journal of nanotechnology* **5**(1), 44–67.

Meyer, E. E., Rosenberg, K. J. and Israelachvili, J. (2006) Recent progress in understanding hydrophobic interactions. *Proceedings of the National Academy of Sciences* **103**(43), 15739–15746.

Monz, J., van der Vliet, D. F., Yanson, A. and Rodriguez, P. (2016) Elucidating the degradation mechanism of the cathode catalyst of pefcs by a combination of electrochemical methods and x-ray fluorescence spectroscopy. *Phys. Chem. Chem. Phys.* **18**, 22407–22415.

Muradov, N. and Veziroglu, T. (2005) From hydrocarbon to hydrogencarbon to hydrogen economy. *International Journal of Hydrogen Energy* **30**(3), 225 – 237.

Newman, M. (2003) The structure and function of complex networks. *SIAM Review* **45**(2), 167–256.

Ottino, J. M. and Khakhar, D. V. (2000) Mixing and segregation of granular materials. *Annual Review of Fluid Mechanics* **32**(1), 55–91.

Park, H.-S., Cho, Y.-H., Cho, Y.-H., Jung, C. R., Jang, J. H. and Sung, Y.-E. (2007) Performance enhancement of {PEMFC} through temperature control in catalyst layer fabrication. *Electrochimica Acta* **53**(2), 763 – 767.

Parker, J. L., Claesson, P. M. and Attard, P. (1994) Bubbles, cavities, and the long-ranged attraction between hydrophobic surfaces. *The Journal of Physical Chemistry* **98**(34), 8468–8480.

Pastor-Satorras, R. and Vespignani, A. (2001) Epidemic spreading in scale-free networks. *Phys. Rev. Lett.* **86**, 3200–3203.

Pauling, L. (1960) *The Nature of the Chemical Bond and the Structure of Molecules and Crystals: An Introduction to Modern Structural Chemistry*. Cornell University Press.

Peng, Z., Doroodchi, E. and Evans, G. (2010) Dem simulation of aggregation of suspended nanoparticles. *Powder Technology* **204**(1), 91–102.

Podczeck, F. and Mia, Y. (1996) The influence of particle size and shape on the angle of internal friction and the flow factor of unlubricated and lubricated powders. *International Journal of Pharmaceutics* **144**(2), 187 – 194.

Podgornik, R. (1989) Electrostatic correlation forces between surfaces with surface specific ionic interactions. *The Journal of Chemical Physics* **91**(9), 5840–5849.

Pollet, B. G. (2010) The use of ultrasound for the fabrication of fuel cell materials. *International Journal of Hydrogen Energy* **35**(21), 11986 – 12004.

Pollet, B. G. and Goh, J. T. (2014) The importance of ultrasonic parameters in the preparation of fuel cell catalyst inks. *Electrochimica Acta* **128**, 292 – 303.

Pratt, L. R. and Chandler, D. (1977) Theory of the hydrophobic effect. *The Journal of Chemical Physics* **67**(8), 3683–3704.

Rein, H. and Spiegel, D. S. (2015) ias15: a fast, adaptive, high-order integrator for gravitational dynamics, accurate to machine precision over a billion orbits. *Monthly Notices of the Royal Astronomical Society* **446**(2), 1424–1437.

Rein, H. and Tamayo, D. (2015) whfast: a fast and unbiased implementation of a symplectic wisdom–holman integrator for long-term gravitational simulations. *Monthly Notices of the Royal Astronomical Society* **452**(1), 376–388.

Rein, H. and Tremaine, S. (2011) Symplectic integrators in the shearing sheet. *Monthly Notices of the Royal Astronomical Society* **415**(4), 3168–3176.

Rein, H. and Liu, S.-F. (2012) Rebound: an open-source multi-purpose n-body code for collisional dynamics. *A&A* **537**, A128.

Riley, C. M., Rose, W. I. and Bluth, G. J. (2003) Quantitative shape measurements of distal volcanic ash. *Journal of Geophysical Research: Solid Earth* **108**(B10).

Roduner, E. (2006) Size matters: why nanomaterials are different. *Chem. Soc. Rev.* **35**, 583–592.

Rolland, T., Tasan, M., Charloteaux, B., Pevzner, S. J., Zhong, Q., Sahni, N., Yi, S., Lemmens, I., Fontanillo, C., Mosca, R., Kamburov, A., Ghiassian, S. D., Yang, X., Ghamsari, L., Balcha, D., Begg, B. E., Braun, P., Brehme, M., Broly, M. P., Carvunis, A.-R., Convery-Zupan, D., Corominas, R., Coulombe-Huntington, J., Dann, E., Dreze, M., Dricot, A., Fan, C., Franzosa, E., Gebreab, F., Gutierrez, B. J., Hardy, M. F., Jin, M., Kang, S., Kiros, R., Lin, G. N., Luck, K., MacWilliams, A., Menche, J., Murray, R. R., Palagi, A., Poulin, M. M., Rambout, X., Rasla, J., Reichert, P., Romero, V., Ruyssinck, E., Sahalie, J. M., Scholz, A., Shah, A. A., Sharma, A., Shen, Y., Spirohn, K., Tam, S., Tejeda, A. O., Trigg, S. A., Twizere, J.-C., Vega, K., Walsh, J., Cusick, M. E., Xia, Y., Barabsi, A.-L., Iakoucheva, L. M., Aloy, P., Rivas, J. D. L., Tavernier, J., Calderwood, M. A., Hill, D. E., Hao, T., Roth, F. P. and Vidal, M. (2014) A proteome-scale map of the human interactome network. *Cell* **159**(5), 1212 – 1226.

Saberi, A. A. (2015) Recent advances in percolation theory and its applications. *Physics Reports* **578**, 1–32.

Sadeghi, E., Putz, A. and Eikerling, M. (2014) Effects of ionomer coverage on agglomerate effectiveness in catalyst layers of polymer electrolyte fuel cells. *Journal of Solid State Electrochemistry* **18**(5), 1271–1279.

Schwarz, D. H. and Djilali, N. (2007) 3d modeling of catalyst layers in pem fuel cells effects of transport limitations. *Journal of the Electrochemical Society* **154**(11), B1167–B1178.

Scott, D. S. (2008) *Smelling land: the hydrogen defense against climate catastrophe*. Queen's Printer Publishing.

Secanell, M., Karan, K., Suleman, A. and Djilali, N. (2007) Multi-variable optimization of pemfc cathodes using an agglomerate model. *Electrochimica Acta* **52**(22), 6318–6337.

Secanell, M., Karan, K., Suleman, A. and Djilali, N. (2008) Optimal design of ultralow-platinum pemfc anode electrodes. *Journal of the Electrochemical Society* **155**(2), B125–B134.

Shao-Horn, Y., Sheng, W. C., Chen, S., Ferreira, P. J., Holby, E. F. and Morgan, D. (2007) Instability of supported platinum nanoparticles in low-temperature fuel cells. *Topics in Catalysis* **46**(3), 285–305.

Sharma, R. and Andersen, S. M. (2018) Zoom in catalyst/ionomer interface in polymer electrolyte membrane fuel cell electrodes: Impact of catalyst/ionomer dispersion media/solvent. *ACS Applied Materials & Interfaces* **10**(44), 38125–38133.

Shibayama, M., Matsunaga, T., Kusano, T., Amemiya, K., Kobayashi, N. and Yoshida, T. (2014) Sans studies on catalyst ink of fuel cell. *Journal of Applied Polymer Science* **131**(3).

Shin, S.-H., Chung, S., Sanii, B., Comolli, L. R., Bertozzi, C. R. and De Yoreo, J. J. (2012) Direct observation of kinetic traps associated with structural transformations leading to multiple pathways of s-layer assembly. *Proceedings of the National Academy of Sciences* **109**(32), 12968–12973.

Shin, S.-J., Lee, J.-K., Ha, H.-Y., Hong, S.-A., Chun, H.-S. and Oh, I.-H. (2002) Effect of the catalytic ink preparation method on the performance of polymer electrolyte membrane fuel cells. *Journal of Power Sources* **106**(12), 146 – 152.

Shukla, S., Bhattacharjee, S., Weber, A. and Secanell, M. (2017) Experimental and theoretical analysis of ink dispersion stability for polymer electrolyte fuel cell applications. *Journal of The Electrochemical Society* **164**(6), F600–F609.

Siddique, N. and Liu, F. (2010) Process based reconstruction and simulation of a three-dimensional fuel cell catalyst layer. *Electrochimica Acta* **55**(19), 5357–5366.

Singh, R., Akhgar, A., Sui, P., Lange, K. and Djilali, N. (2014) Dual-beam fib/sem characterization, statistical reconstruction, and pore scale modeling of a pemfc catalyst layer. *Journal of The Electrochemical Society* **161**(4), F415–F424.

Singh, R., Sui, P., Wong, K., Kjeang, E., Knights, S. and Djilali, N. (2018) Modeling the effect of chemical membrane degradation on pemfc performance. *Journal of The Electrochemical Society* **165**(6), F3328–F3336.

Soboleva, T., Zhao, X., Malek, K., Xie, Z., Navessin, T. and Holdcroft, S. (2010) On the micro-, meso-, and macroporous structures of polymer electrolyte membrane fuel cell catalyst layers. *ACS Applied Materials & Interfaces* **2**(2), 375–384. PMID: 20356182.

Sorensen, C. and Wang, G. (1999) Size distribution effect on the power law regime of the structure factor of fractal aggregates. *Physical Review E* **60**(6), 7143.

Stokes, R. J. and Evans, D. F. (1996) *Fundamentals of Interfacial Engineering (Advances in Interfacial Engineering Series)*. Wiley-VCH.

Synodis, M. J., Porter, C. L., Vo, N. M., Reszka, A. J., Gross, M. D. and Snyder, R. C. (2013) A model to predict percolation threshold and effective conductivity of infiltrated electrodes for solid oxide fuel cells. *Journal of The Electrochemical Society* **160**(11), F1216–F1224.

Tadmor, R., Hernandez-Zapata, E., Chen, N., Pincus, P. and Israelachvili, J. N. (2002) Debye length and double-layer forces in polyelectrolyte solutions. *Macromolecules* **35**(6), 2380–2388.

Takahashi, I. and Kocha, S. S. (2010) Examination of the activity and durability of {PEMFC} catalysts in liquid electrolytes. *Journal of Power Sources* **195**(19), 6312 – 6322.

Teixeira, J. (1988) Small-angle scattering by fractal systems. *Journal of Applied Crystallography* **21**(6), 781–785.

Turner, J. A. (2004) Sustainable hydrogen production. *Science* **305**(5686), 972–974.

Tyrrell, J. W. and Attard, P. (2001) Images of nanobubbles on hydrophobic surfaces and their interactions. *Physical Review Letters* **87**(17), 176104.

Walz, J. Y. and Sharma, A. (1994) Effect of long range interactions on the depletion force between colloidal particles. *Journal of colloid and interface science* **168**(2), 485–496.

Wilson, M. S. and Gottesfeld, S. (1992) Thin-film catalyst layers for polymer electrolyte fuel cell electrodes. *Journal of Applied Electrochemistry* **22**(1), 1–7.

Wisdom, J. and Holman, M. (1991) Symplectic maps for the n-body problem. *The Astronomical Journal* **102**, 1528–1538.

Wu, T. and Djilali, N. (2012) Experimental investigation of water droplet emergence in a model polymer electrolyte membrane fuel cell microchannel. *Journal of Power Sources* **208**, 248–256.

Wu, X., Wang, X., He, G. and Benziger, J. (2011) Differences in water sorption and proton conductivity between nafion and speek. *Journal of Polymer Science Part B: Polymer Physics* **49**(20), 1437–1445.

Xiao, Y., Dou, M., Yuan, J., Hou, M., Song, W. and Sundn, B. (2012) Fabrication process simulation of a pem fuel cell catalyst layer and its microscopic structure characteristics. *Journal of The Electrochemical Society* **159**(3), B308–B314.

Xie, Z., Zhao, X., Adachi, M., Shi, Z., Mashio, T., Ohma, A., Shinohara, K., Holdcroft, S. and Navessin, T. (2008) Fuel cell cathode catalyst layers from "green" catalyst inks. *Energy Environ. Sci.* **1**, 184–193.

Xing, L., Hossain, M. A., Tian, M., Beauchemin, D., Adjemian, K. T. and Jerkiewicz, G. (2014) Platinum electro-dissolution in acidic media upon potential cycling. *Electrocatalysis* **5**(1), 96–112.

Xu, F., Zhang, H., Ilavsky, J., Stanciu, L., Ho, D., Justice, M. J., Petrache, H. I. and Xie, J. (2010) Investigation of a catalyst ink dispersion using both ultra-small-angle x-ray scattering and cryogenic tem. *Langmuir* **26**(24), 19199–19208.

Yan, Y., Huang, J. and Tang, B. Z. (2016) Kinetic trapping–a strategy for directing the self-assembly of unique functional nanostructures. *Chemical Communications* **52**(80), 11870–11884.

Yoshida, H. (1992) Symplectic integrators for hamiltonian systems: Basic theory. *Chaos, Resonance and Collective Dynamical Phenomena in the Solar System* **152**, 407.

Zhang, J. (2008) *PEM Fuel Cell Electrocatalysts and Catalyst Layers: Fundamentals and Applications*. Springer.

Zook, J. M., MacCuspie, R. I., Locascio, L. E., Halter, M. D. and Elliott, J. T. (2011) Stable nanoparticle aggregates/agglomerates of different sizes and the effect of their size on hemolytic cytotoxicity. *Nanotoxicology* **5**(4), 517–530.